

Master Degree course in Automotive Engineering

Master Degree Thesis

Comparative Design and Thermal Performance of Stator Cooling Strategies for a High-Speed Electrically-Excited Synchronous Machine (EESM)

Supervisors

Prof. Andrea TONOLI Prof. Vittorio RAVELLO

> Candidate Lorenzo PINNISI

ACADEMIC YEAR 2025-2026

Acknowledgements

To all the important people in my life.

Abstract

The present work investigates and compares three stator cooling configurations for a high-speed, cost-effective Electrically Excited Synchronous Motor (EESM) for automotive application. Starting from a lumped thermal model in MotorCAD to retriever losses and heat distribution, three stator forced liquid cooling solutions were designed: (I) Housing Water-Jacket (WJ), (II) Direct-Slot with in-slot flow (DirectSlotV1), and (III) Direct-Slot with in-slot flow plus stator ducts (DirectSlotV2). The geometries were then defined in SolidWorks and SpaceClaim and solved numerically in Ansys Fluent considering a steady-state non-isothermal flow. A 50/50 EGW oil coolant was used with an inlet temperature of 65 C and four different flow rates (6, 10, 15 and $18 \ l/min$) were tested under the same thermal setup and conditions provided by MotorCAD. The performance of the solution was evaluated via channel pressure drop, and the maximum reached stator temperature. All three solutions meet the limit of temperature imposed for continuous operation, but DirectSlotV2 provides the best trade-off between cooling performance, pressure drop, and cost-effectiveness. The study outlines the modeling assumptions and limitations, and provides a solid foundation for future studies.

Contents

Li	st of	Figure	es	5
\mathbf{Li}	st of	Tables	; ;	7
1	Intr	oducti	on	9
	1.1	Motiva	ation	10
	1.2	Object	ive	10
	1.3	Struct	ure of the thesis	11
2	The	EV M	farket	13
	2.1	Electri	c vehicle market	13
		2.1.1	Global electric car sales, 2025 data	13
	2.2	Electri	c two and three-wheelers and light commercial vehicles (LCVs) $$	14
	2.3	Global	availability and size trends	15
		2.3.1	Affordability and total cost of ownership (TCO)	15
	2.4		g range evolution	15
	2.5	Overvi	ew	16
3	\mathbf{EM}	Typol	ogies overview	17
	3.1	AC Ele	ectrical Machines	17
	3.2	·	ronous Machines	18
	3.3	Synchr	ronous Machines typologies	19
		3.3.1	Wound Rotor Synchronous Machine (WRSM)	20
		3.3.2	Synchronous Reluctance Machine	23
		3.3.3	Permanent Magnet Synchronous Machine (PMSM)	25
		3.3.4	SMs characteristics summary	25
		3.3.5	WRSMs main applications	26
4			ly Excited Synchronous Motor (EESM) in traction applica-	
	tion			27
	4.1	Featur	es of EESMs	27
		4.1.1	Advantages	28
		4.1.2	Disadvantages	29
	4.2		in the automotive market	29
		4.2.1	Renault ZOE	29

	4.2.2 Renault Megane E-tech
	4.2.3 BMW - i4/iX Series
	4.2.4 BYD Seal Excellence
	4.2.5 ZF
	4.2.6 Comparative Overview
4.	B EESM design for high-speed and cost-effective for a <i>Stellantis</i> traction
	application
4.	4 Rotor Pole Number
4.	5 Stator windings
4.	6 Winding insulation
4.	7 Supply System
4.	8 Cooling System
5 C	FD: Computational Fluid Dynamics
5.	1 CFD generic structure
5.	2 Governing equations
	5.2.1 Reynolds Transport Theorem (RTT)
	5.2.2 Mass Conservation (Continuity equation)
	5.2.3 Momentum Conservation (NSE)
	5.2.4 Energy Conservation Equation
	5.2.5 Coupling of the equations
5.	3 Governing equations solving methods
5.	4 Heat transfer
5.	
	5.5.1 Conduction
	5.5.2 Convection
	5.5.3 Radiation
6 St	ator Cooling systems for high speed and torque/density motors
6.	G G G G G G G G G G G G G G G G G G G
6.	1 0
6.	
6.6	1 0
	6.4.1 Housing Water Jacket Cooling
	6.4.2 Direct Slot Cooling
	6.4.3 Oil-flooded Cooling
	6.4.4 End-tip Cooling
	6.4.5 Oil-spray Cooling
7 E	ESM prototype design (MotorCAD)
7.	
	7.1.1 Water Jacket Cooling
	7.1.2 Direct Slot Cooling with In-slot winding cooling
	7.1.3 Direct Slot Cooling with In-slot winding cooling and stator ducts .
7	2. Losses computation (MotorCAD)

8	\mathbf{Met}	hodolo	ogy	63
	8.1	Geome	etry definition - SolidWorks	63
	8.2	Geome	etry description - SpaceClaim	64
	8.3	CFD a	nalysis - Ansys Fluent	65
		8.3.1	Mesh generation	65
		8.3.2	Pre-processing: solver settings	66
		8.3.3	Convergence criteria	67
		8.3.4	Mesh dependence analysis	
9	Resi	ults an	nd discussion	71
	9.1	Analyt	tical comparison	71
	9.2		ical comparison	
10	Con	clusior	1	77
Bi	bliog	raphy		79

List of Figures

1.1	SM structure EESM (left) and PMSM (right)	0
2.1	Global electric car stock trends, 2014-2024 [1]	.3
2.2	Quarterly electric car sales, 2021-2025 [1]	4
2.3	BEVs battery range by segment 2015-2023 [1]	.5
3.1	AC machines classification based on excitation method and magnetic flux direction	.8
3.2	Synchronous machine typologies [2]	9
3.3		20
3.4		21
3.5	Isotropic rotor of a SM [4]	22
3.6		23
3.7		24
3.8	Geometry and torque generation of a SyRM	24
3.9	Geometry and torque generation of a PMSM	25
3.10	Summary of motor types and characteristics [3]	26
4.1	EESM wounded rotor structure (MotorCAD)	28
4.1 4.2	(28 30
	Renault Zoe vehicle and EESM architecture [5]	
4.2	Renault Zoe vehicle and EESM architecture [5]	3 0
4.2 4.3	Renault Zoe vehicle and EESM architecture [5]	30 30
4.2 4.3 4.4	Renault Zoe vehicle and EESM architecture [5]	30 30 31
4.2 4.3 4.4 4.5 4.6 4.7	Renault Zoe vehicle and EESM architecture [5]	30 30 31 34 34
4.2 4.3 4.4 4.5 4.6	Renault Zoe vehicle and EESM architecture [5]	30 30 31 34
4.2 4.3 4.4 4.5 4.6 4.7	Renault Zoe vehicle and EESM architecture [5]	30 31 34 34 35
4.2 4.3 4.4 4.5 4.6 4.7 4.8	Renault Zoe vehicle and EESM architecture [5]	30 31 31 34 35
4.2 4.3 4.4 4.5 4.6 4.7 4.8 5.1	Renault Zoe vehicle and EESM architecture [5]	30 31 34 34 35
4.2 4.3 4.4 4.5 4.6 4.7 4.8 5.1 5.2 5.3	Renault Zoe vehicle and EESM architecture [5]	30 30 31 31 34 35 42 45
4.2 4.3 4.4 4.5 4.6 4.7 4.8 5.1	Renault Zoe vehicle and EESM architecture [5]	30 31 34 34 35
4.2 4.3 4.4 4.5 4.6 4.7 4.8 5.1 5.2 5.3	Renault Zoe vehicle and EESM architecture [5]	30 30 31 31 34 35 42 45

6.3	Ventilation on EFC (left) and OFC (right) motor	52
6.4	Housing Water Jacket cooling solutions: zigzag (left) and spiral (right) [12]	53
6.5	Direct Slot Cooling with sleeve and axial ducts [13]	53
6.6	Oil-flooded stator of an axial-flux motor [14]	54
6.7	End-tip cooling method schematic	54
6.8	Oil spray cooling in different configurations: nozzle on top of the end-	
	winding (left) and through the hollow shaft (right) $[15]$	55
7.1	3D view of the EESM in MotorCAD	57
7.2	Thermal network base round housing configuration	59
7.3	Thermal network WJ cooling configuration	60
7.4	Direct Slot with In-slot winding cooling configuration	60
7.5	Direct Slot with In-slot winding cooling and stator ducts configuration	61
8.1	3D model of WJ cooling (left), DirectSlotV1 (center), and DirectSlotV2 (right)	64
8.2	Assignment of domain parts in SpaceClaim, case of WJ cooling	65
8.3	WJ mesh model discretization	66
8.4	Mesh dependence analysis concerning the impact on Heat Transfer Coefficient and on the average coolant temperature in the channel for WJC	
	strategy at fixed parameters and gradually increasing the mesh refinement	68
9.1	Pressure drop vs volumetric flow rate for each cooling strategy	72
9.2	Maximum temperature vs volumetric flow rate for each cooling strategy .	72
9.3	Outlet coolant temperature vs volumetric flow rate for each cooling strategy	73
9.4	Heat extraction from stator core vs volumetric flow rate for each cooling	
	strategy	73
9.5	WJ stator core and housing temperature distribution varying the volumet-	
	ric flow rate	74
9.6	DirectSlotV1 stator core and housing temperature distribution varying the	
	volumetric flow rate	75
9.7	DirectSlotV2 stator core and housing temperature distribution varying the	
	volumetric flow rate	75

List of Tables

4.1	Comparative technical data of EV with EESMs in the market	32
4.2	Initial data specifications for the EESM prototype	33
7.1	Stator and rotor geometric input data from Motor-CAD	58
7.2	Losses contributions calculated by MotorCAD, in continuous mode	61
8.1	Bill of Materials (BOM) used for simulation	67
8.2	Characteristic element size in the the main regions for five models with	
	different total number of cells	68

Chapter 1

Introduction

"Today, vehicle electrification has become an interesting research direction for the automotive industry and the academic community. The applications of electric drives in the automotive industry include electric propulsion, electric power steering, and inwheel drive" [16].

The asynchronous machine has long been the preferred choice for electric automotive propulsion. However, the increasing demand for higher efficiency in recent years has prompted a shift towards the adoption and further study of synchronous machines (SMs). Synchronous motors are widely used in the industry because of their ability to maintain a constant rotational speed regardless of the level of the applied load. The constant speed is achieved by synchronizing the rotor with the frequency of the electric alternating current connected to the motor. This leads to the immediate consequence that this kind of electric motor generates heat and needs to be cooled to avoid overheating. Among these electric typologies, the Permanent Magnet Synchronous Machine (PMSM) and the Externally Excited Synchronous Machine (EESM) have gained particular attention due to their superior performance in meeting modern efficiency standards. This document will focus on Electrically Excited Synchronous Motors (EESMs) which gained popularity in electric applications because of their inherent benefits.

EESMs use field windings in the rotor for excitation, unlike PMSMs, which rely on permanent magnets. This provides the advantage of controlling the rotor field current, allowing motor adjustment across various operating points. As a result, EESM control is crucial for optimizing efficiency and reliability, especially in applications such as electric vehicles, industrial drives, and renewable energy systems, where torque and speed are key factors. The synchronous machine offers benefits such as high efficiency, power density, and torque at startup. In contrast, PMSMs have a constant rotor magnetization due to their permanent magnets, whereas EESMs offer greater flexibility with an additional degree of freedom in the excitation current. The basic electric structure of SMs is shown in Figure 1.1.

While operating, as previously specified, electric motors generate heat mainly due to electromagnetic and mechanical losses occurring within their components. Effective thermal management is therefore essential to prevent local overheating, materials, and

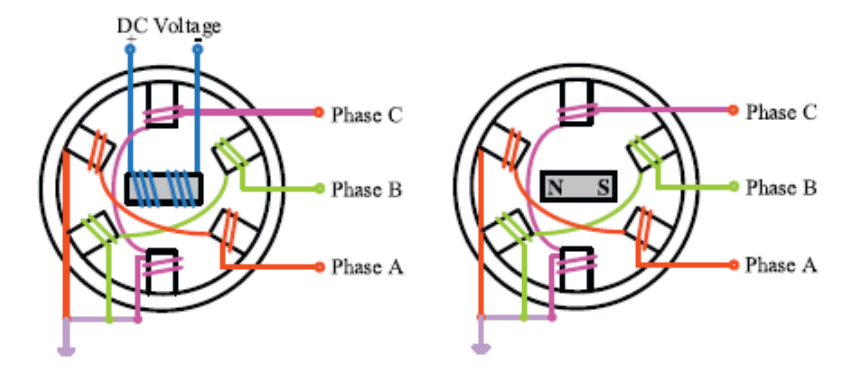


Figure 1.1. SM structure EESM (left) and PMSM (right)

performance degradation. Furthermore, excessive temperatures can accelerate insulation aging, alter magnetic properties, and increase electrical resistance, leading to further energy losses and possible failures. For this reason, developing efficient cooling strategies is crucial to ensure optimal performance, reliability, and durability of electric machines.

1.1 Motivation

The growing demand for electric motors in high-performance applications requires advanced control solutions that address both torque regulation and effective cooling strategies to ensure optimal thermal management and overall efficiency. Some traditional cooling strategies, such as water jacket cooling, are cost-effective and well-proven; however, they may become inadequate when dealing with the higher rotational speeds and variable load conditions demanded by modern applications.

To address these challenges, several cooling approaches have been developed, each with its own advantages and limitations. Passive cooling represents an economical solution, as it relies on the motor housing to dissipate heat by natural convection, but is heavily influenced by material properties and geometry, and offers, consequently, a limited heat transfer capability. Active cooling instead improves heat dissipation through forced air, liquid circulation, or phase-change systems, and thus provides higher convective efficiency, but at the cost of increased system complexity, possible friction losses, electrical faults, corrosion risks, and higher pump power consumption.

This work aims to analyze different forced-liquid cooling strategies for the stator of an EESM. Starting from lumped-parameter thermal models, these strategies will be validated and/or questioned through CFD simulations conducted in Ansys Fluent, to identify the most effective cooling configuration for the prototype under study.

1.2 Objective

The objective of the thesis is to analyze and optimize cooling strategies for a high-speed wound rotor synchronous motor (EESM) prototype using a direct liquid cooling system

for the stator in order to:

- Compare the different configurations and evaluate their impact on efficiency, thermal performance, and reliability under continuous mode operating condition;
- Validate thermal models through CFD simulations using Ansys Fluent to predict thermal behavior and select the best cooling system design;
- Identify the most promising solutions for improving thermal management for automotive and industrial applications.

The comparison was conducted under controlled conditions, ensuring that factors such as flow rate, external parameters, the chosen cooling liquid, and the geometries of the CAD model remain consistent in all simulations. Note that certain simplifications were made in the models and parameters used, which are justified given the project's current stage in the prototyping phase. The intention is to create a solid foundational understanding that can guide future optimizations, for further refinement and adjustments as the design progresses.

1.3 Structure of the thesis

- Literature Review
- Theoretical Framework
- Model creation
- Simulation and Analysis
- Results and Discussion
- Conclusion and Future Work

Chapter 2

The EV Market

2.1 Electric vehicle market

"The Global EV Outlook is an annual publication of the IEA (International Energy Agency) that identifies and assesses recent developments in electric mobility across the globe. It is developed with the support of members of the Electric Vehicles Initiative (EVI) and provides comprehensive data and insights on EV adoption, market trends, and policy developments worldwide" [2]. The "Global EV Outlook 2025" [1] is useful to analyze the current state and future trends of the global EV market and more specifically of the global electric vehicle market, the focus of this work.

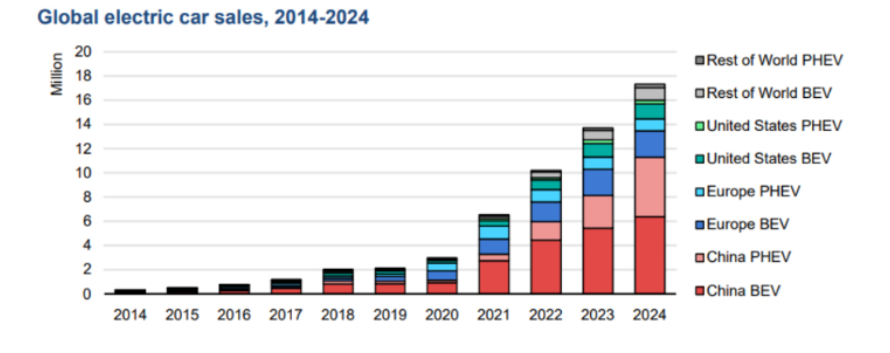


Figure 2.1. Global electric car stock trends, 2014-2024 [1]

2.1.1 Global electric car sales, 2025 data

According to the latest IEA Global Energy Review 2025 [1], global sales of electric cars exceeded 17 million units in 2024, with a growth rate of more than 25% compared to the previous year. Electric vehicles (EVs) represented more than 20% of total car sales worldwide, with the majority of these sales concentrated in China, which alone represented almost two-thirds of global electric car sales; Europe follows, with approximately 20%, along with the United States, where the market share exceeded 10%, as shown in

Fig. 2.2

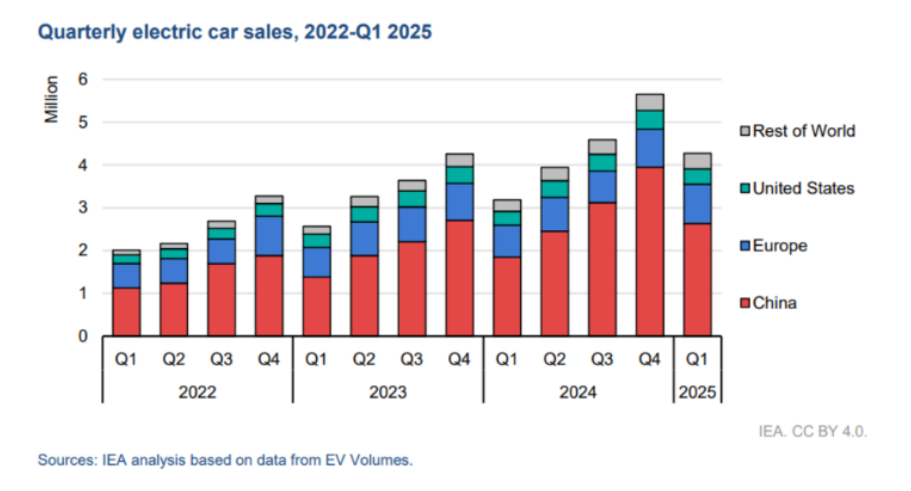


Figure 2.2. Quarterly electric car sales, 2021-2025 [1]

China increased car sales by nearly 40%, primarily due to the rise of plug-in hybrid vehicles (PHEVs), which increased by 80%, while battery electric vehicles (BEVs) expanded by around 20%. The United States recorded an increas of more than 10 %, driven by the introduction of new models and federal tax incentives. Conversely, the European Union, saw a 6% decline, primary due to Germany's abrupt termination of EV purchase at the end of 2023. Outside of the main markets, emerging economies such as Brazil and Indonesia saw a surge in EV by 140% and 190% respectively.

2.2 Electric two and three-wheelers and light commercial vehicles (LCVs)

Two- and three-wheelers continue to play a significant role in emerging economies; the largest markets remain India, China, and the ASEAN region, when affordability and practicality drive their adoption. However, electrification is expanding rapidly in these segments, as this vehicle typology serves as an accessible entry point to clean mobility for lower-income consumers.

The market for electric light commercial vehicles also expanded in 2024, with an increase in global sales of more than 50%. China and Europe led this growth, driven by the electrification of urban delivery fleets and the introduction of stricter emission standards for city logistics.

2.3 Global availability and size trends

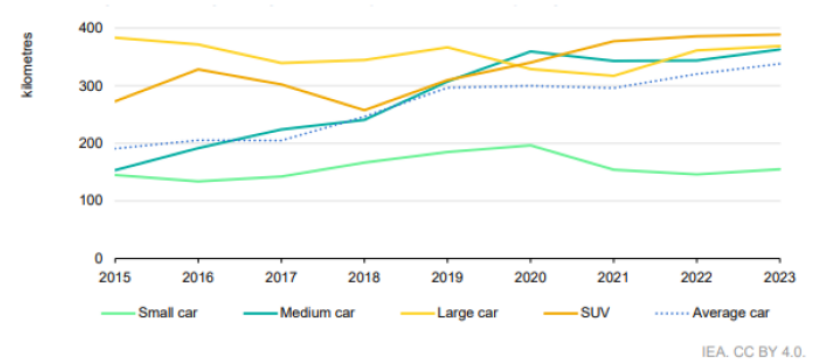
The range of available electric models continued to grow in 2024, showing a preference for larger vehicles. In leading markets such as the United States, around two-thirds of newly launched electric models were SUVs or pick-up trucks, while small cars represented only about 25% of battery electric vehicle sales. In Europe, small and medium models represented roughly 40% and in China about 50%, indicating greater interest of the consumer in compact and affordable options.

2.3.1 Affordability and total cost of ownership (TCO)

The trend remained generally the same, since the upfront cost of electric costs is higher than that of internal combustion engine (ICE) vehicles, while the total cost of ownership continues to decline, supported by lower fuel and maintenance expenses. Furthermore, the price gap between EVs and conventional cars narrowed further in 2024, thanks to declining battery costs, competitive manufacturing, and scale economics. China remains the global benchmark for affordable electric cars, while in Europe and in the US, the same price is projected to be achieved between 2025 and 2028, particularly in smaller segments.

2.4 Driving range evolution

Technological development has recently led to a moderate increase in driving range, as the sales-weighted average range of BEVs has increased by approximately 75% since 2015. However, especially for small urban models with an average of approximately 150 km, EVs range appears just "sufficient" for daily commuting. Larger models now commonly exceed 350-400 km, reflecting improvements in battery capacity and vehicle design, although it still brings to light what is, for now, the soft underbelly of this new technology.



Notes: SUV = sports utility vehicle. Range in kilometres calculated using global weighted average fuel economy (Worldwide Harmonised Light Vehicle Test Procedure [WLTP]) and battery capacity by size segment. Fuel economy reflects on-road conditions by applying a factor of 1.1. Small cars include A and B segments. Medium cars include C and D segments, and A segments with SUV body type. Large cars include E and F segments, multi-purpose vehicles and B segments with SUV body type. SUV category in figure encompasses segments C to F with SUV body type.

Source: IEA analysis based on data from EV Volumes.

Figure 2.3. BEVs battery range by segment 2015-2023 [1]

2.5 Overview

Overall, the IEA highlights the electro-mobility transition and extensions, as it is no longer confined to a few leading regions. Although China remains the dominant force, new markets are rapidly emerging, with EV sales outside major economies growing by more than 50% in 2024. These dynamics indicate that global electric mobility is no longer limited to a small segment of early adopters or high-income markets. The transition now encompasses a wide spectrum of vehicle categories, from private passenger cars to public transport fleets, commercial delivery vans, and even two- and three-wheelers commonly used in emerging economies. This progressive diversification demonstrates that electrification is evolving into a comprehensive mobility ecosystem rather than a single-product innovation. The electric vehicle is becoming more accessible, technologically advanced, and supported by expanding charging infrastructures; the shift toward electric mobility reflects a structural transformation of the global transport system, integrating environmental goals, industrial competitiveness, and consumer demand with a unified objective of sustainable growth.

Chapter 3

EM Typologies overview

3.1 AC Electrical Machines

AC machines are motors that convert AC electric energy to mechanical energy and generators that convert mechanical energy to electric energy.

AC machines differ from dc machines by having their armature windings almost always located on the stator while their field windings are located on the rotor. A set of three-phase ac voltages is induced into the stator armature windings of an ac machine by the rotating magnetic field from the rotor field windings (generator action). "Conversely, a set of three-phase currents flowing in the stator armature windings produces a rotating magnetic field within the stator. This magnetic field interacts with the magnetic rotor magnetic field to produce the torque in the machine (motor action)" [17]. The focal operational principle of ac machine operation is that a three-phase set of currents, flowing in an armature windings, each of equal magnitude and phase-shafted by 120 C, produces a rotating magnetic field of constant magnitude.

The two main classes of ac machines are **synchronous machines** and **induction machines**. Whether a motor or a generator is considered, the field current of synchronous machines is supplied by a separate dc power source, while the field current of induction machines is supplied by magnetic induction (transformer action) into the field windings.

Moreover, AC motors can be classified based on the excitation method (to generate the magnetic flux):

- Induction and synchronous reluctance machines: These use multi-phase stator windings to create time-shifted AC voltages and currents.
- Wound rotor synchronous machines: These feature a rotor with DC windings, energized through brushes and slip rings.
- Permanent magnet synchronous machines (PMSM): The rotor contains permanent magnets that generate the magnetic field.

Furthermore, the magnetic flux direction further categorizes machines (Fig. 3.1):

- Radial flux machines: These machines typically have an external stator and internal rotor, commonly seen in rotating machines.
- Axial flux machines: These feature a disc-shaped rotor with axial alignment between stator and rotor.
- **Planar flux machines**: These include linear and tubular machines, often used in specialized applications.

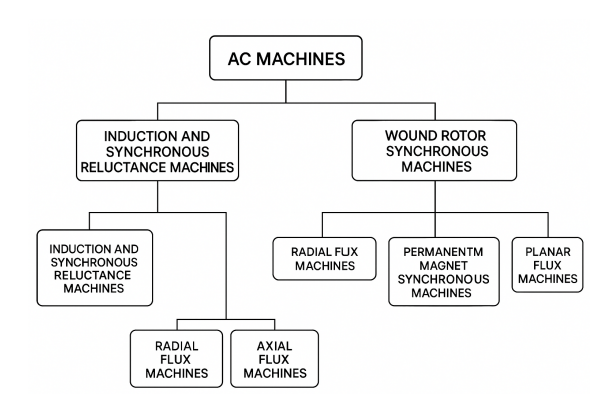


Figure 3.1. AC machines classification based on excitation method and magnetic flux direction

Despite the different designs, all of these machines rely on the interaction of magnetic fields and electrical current to generate torque. The main differences lie in how the current is applied and the magnetic flux is controlled.

3.2 Synchronous Machines

Synchronous machines are used in a variety of applications, from low-power devices as clocks and timing motors to electric power generation, with output capacities exceeding 1500 MW.

A particular benefit of this type of machine is that synchronous motors operate at constant speed regardless of load variations, i.e, rotor always rotates at the same speed as the rotating magnetic field generated by the stator, crucial for applications that require high-speed stability, such as machine tools and conveyor systems. These motors exhibit high energy efficiency, particularly at partial load, reducing energy losses. Furthermore, they are capable of handling temporary overloads without compromising performance due to their robust construction. However, synchronous motors are not self-starting, so they require external systems such as starting motors or inverters to reach the synchronous speed, consequently increasing complexity and cost. They are also sensitive to load changes, which can affect performance, and their initial cost is higher compared to asynchronous motors.

3.3 Synchronous Machines typologies

A synchronous machine operates at a fixed speed determined by the frequency of the power supply connected to it. This operating speed of the machine, known as the **synchronous speed**, which represents the rotational speed of the magnetic field, is given by the equation:

$$\Omega_s = \frac{(60 * f)}{P_p} \tag{3.1}$$

where f is the supply voltage frequency and P_p is the number of pairs of poles. In AC synchronous machines, the mechanical speed of the rotor matches the synchronous speed, with the torque always flowing through the stator windings as the rotor stays locked in synchrony with the field, turning at the synchronous speed mentioned before.

The main types of synchronous electrical machine family are:

- Separately Excited Synchronous machines (SMs);
- Synchronous Reluctance machines (SyRMs);
- Permanent Magnet Synchronous machines (PMSMs)

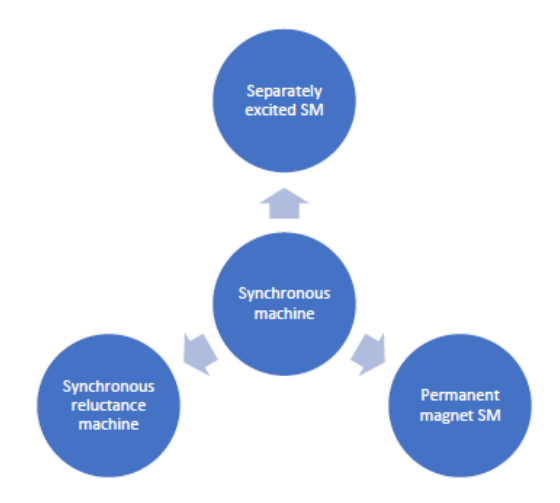


Figure 3.2. Synchronous machine typologies [2]

For synchronous machines, regardless of the stator winding configuration (distributed/concentrated), the rotor design imposes the motor type and name. A wide number of different rotor structures are possible as, just to give an idea: SPM (Surface mounted Permanent Magnet), IPM (Spoke-type or V-type Interior Permanent Magnet), PM-SyR (PM-assisted Synchronous Reluctance) and SyR (Synchronous Reluctance).

Torque generation in SMs The torque produced by the synchronous motor is made up of two components:

- **PM torque**: each stator current produces a torque component in association with the PM magnetic field along the air gap (Lorentz law);
- Reluctance torque: if the rotor is anisotropic, meaning that its inductance varies with position along the air gap, it interacts with the rotating magnetic field produced by the stator. As a result, the rotor experiences a reluctance torque, which makes it tend to align its axis of maximum inductance with the stator magnetic field; the rotor tries always to minimize the magnetic reluctance (i.e. its magnetic energy) in the air gap.

The overall torque in synchronous machines results from the combination of the PM torque and the reluctance torque, whose ratio varies according to the rotor geometry (saliency and magnet configuration), as shown in figure below:

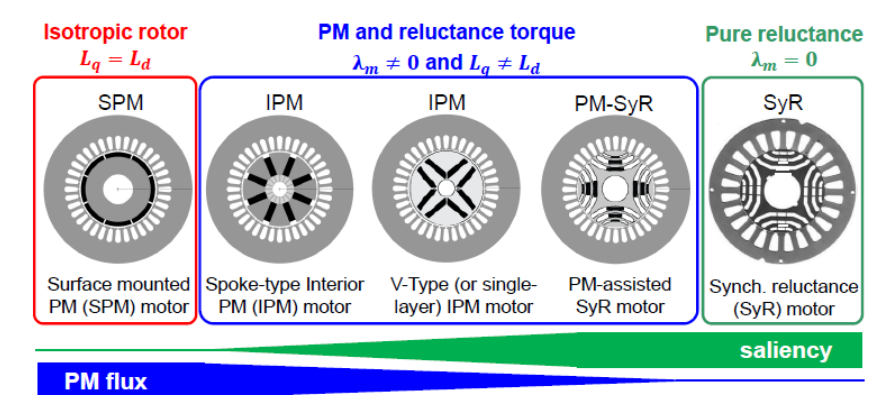


Figure 3.3. Classification of SMs based on saliency and magnet configuration [3]

3.3.1 Wound Rotor Synchronous Machine (WRSM)

The Wound Rotor Synchronous Machine (WRSM), also known as Electrically Excited Synchronous Machine (EESM), belongs to the synchronous machine family, characterized by the fact that the rotor rotates at exactly the same angular speed produced by the rotating magnetic field (characteristic speed) produced in the air gap.

The stator consists of a three-phase winding, most commonly connected in a star configuration. The stator acts as the armature, and thus, within its windings, the electromotive force (EMF) is induced. The rotor, often known as the field or excitation system, serves as the main source of magnetic flux. The field windings (rotor) are supplied by an external DC source, typically through slip rings and brushes, although contactless excitation systems are in continuous expansion.

From a magnetic and structural point of view, the stator is made up of laminated stacked sheets of electrical steel (back iron). These sheets are arranged orthogonally to

the machine's rotational axis and generally have a standard thickness of around 0.5 mm, to minimize eddy current losses caused by the time-varying magnetic field.

The rotor instead, which produces a steady magnetic flux over time due to DC excitation, does not experience relevant alternating magnetic fields and, therefore, it can be constructed from solid magnetic material rather than laminated steel. Some advanced configurations may also incorporate salient poles or optimized rotor shapes to improve torque-power characteristics.

To conclude, the WRSM/EESM configuration offers a high degree of controllability, as the field current can be precisely adjusted to regulate the machine's torque, voltage, and power factor; features that make this solution particularly suitable for automotive traction systems, power generation, and high performance industrial drives, where dynamic control end efficiency are crucial.

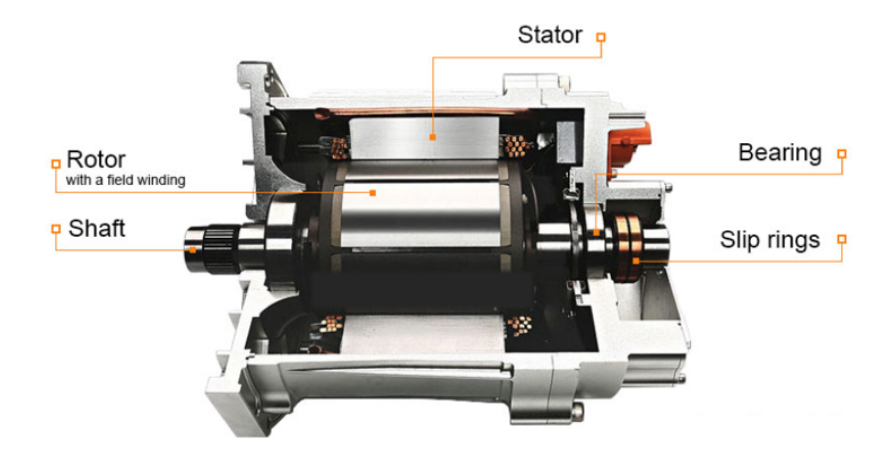


Figure 3.4. EESM example exploded view

Excitation methods

There are two basic ways to magnetize a externally excited machine:

- Slip rings and brushes: field winding on the rotor is supplied with a direct current through slip rings and brushes. The DC supply can come from either a converter or a rotating DC exciter mounted on the shaft. This system is simple and allows direct control of the excitation current, although it requires two sets of brushes, one on the DC exciter and one on the main machine, which are subjected, as a consequence, to high wear and electric losses;
- Brushless excitation: excitation current is supplied without physical contact, thus eliminating the need for brushes and slip rings. This approach reduces maintenance and improves reliability, but an extra electronic control of the excitation

current is needed, increasing the complexity of the machine design. From catalougue, several configurations exist:

- A small synchronous exciter is mounted of the main generator shaft and induces an AC voltage in its rotor armature through the stator field. This voltage is rectified by a rotating rectifier and used to supply the main machine's field winding;
- An axial transformer or wound-rotor induction generator is used to magnetically transfer the power to the rotor circuit, with the field current rectified on the rotating side.

Cylindrical or Salient pole rotor

Based on the technical discussion reported in [4], the rotor can be of two different types:

• Cylindrical rotor (isotropic): characterized by a distributed winding, whose active conductors are housed in slots that cover approximately $\frac{2}{3}$ of the rotor surface. This configuration uses a smooth (cylindrical) rotor, typically used in 2, and occasionally 4-poles machines. Due to its configuration, the air gap remains essentially uniform along the entire periphery of the machine;

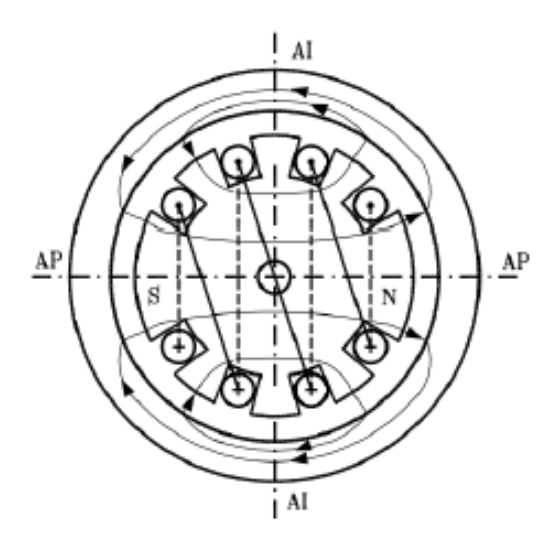


Figure 3.5. Isotropic rotor of a SM [4]

• Salient poles rotor (anisotropic): characterized by concentrated windings, where each pole body is wounded by a coil; all the coils are connected in series, thus the winding direction is inverted pole by pole. Furthermore, "each pole is made by a magnetic structure with a parallelepiped shape (pole body) and it ends with a polar expansion" [2]. Thus, the air gap is variable, as it increases from the pole axis to

both ends of the expansions (technically called "expansion" or "air gap shaping"). This configuration is preferred for SMs with pole number greater than 4.

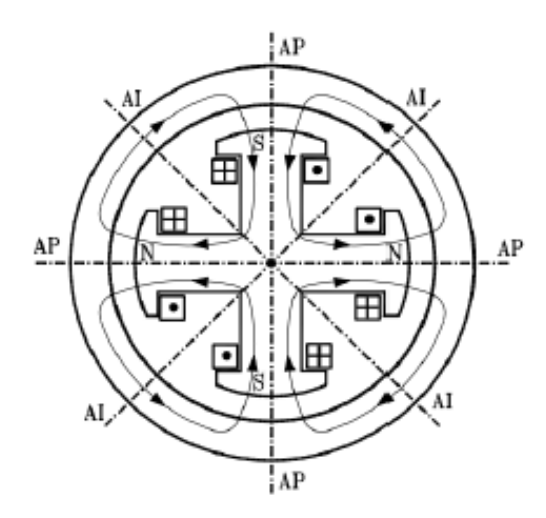


Figure 3.6. Anisotropic 4-pole rotor SM [4]

With the objective to give consistency, below follows the notation used for the rotor symmetry axes, visible in the rotor configurations explained before (Fig. 3.5, Fig. 3.6):

- Polar axis (AP: Asse Polare) or Direct axis (d): this represent the magnetic axis, along which the flux of a pole is directed when only the field winding is energized;
- Interpolar axis (AI: Asse Interpolare) or Quadrature axis (q): this represent the bisector of the directions of the two adjacent polar axes. Since the electrical angle between two consecutive poles is 180 electrical degrees, the interpolar (q) axis lies 90 degress from the polar (d) axis and defines the quadrature direction.

3.3.2 Synchronous Reluctance Machine

A typical synchronous reluctance machine (SynRM or SyRM) operates without permanent magnets, significantly reducing material costs and weight while still providing a good torque density, although at the cost of a lower power factor.

Since only the magnetic saliency of the rotor is exploited, the operation of a SyRM is based on the reluctance effect, thus the torque generation is provided by the ratio between the inductance of the direct and quadrature axes.

The machine's performance therefore strongly depends on the anisotropy ratio, defined as L_d/L_q , where L_d and L_q are respectively the inductance along the direct and the quadrature axes. By definition, the d-axis corresponds to the direction of maximum

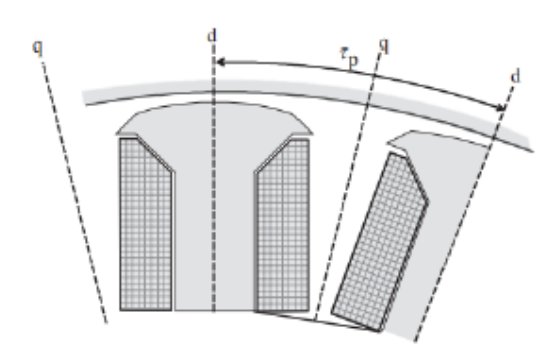


Figure 3.7. Polar (d) and Interpolar (q) axes of a salient-pole SM [4]

inductance, whereas the q-axis corresponds to the direction of minimum inductance. "The objective is to create a maximum inductance difference between the direct and quadrature axes [2]"; in other terms, for a given load angle, the higher the ratio L_d/L_q , the higher the torque and power output of the machine. Consequently, the main design objective is to maximize this inductance ratio through appropriate rotor geometry.

With this aim, the rotor core is made by alternating regions of magnetic steel, which serve as flux guides, and non-magnetic air barriers, known as flux barriers. As a result, one of the optimal configuration is typically obtained when these two regions occupy roughly equal portions of the rotor's cross-section (approximately 50:50), resulting in balanced trade-off between mechanical robustness and magnetic anisotropy. When very high anisotropy ratios are needed, the rotor lamination sheets can be arranged axially along the shaft.

To conclude, to ensure proper operation, this type of electric machine requires coordinated control of the two current components, i_d and i_q , to achieve torque maximization; a typical SyRM machine schematic is shown below:

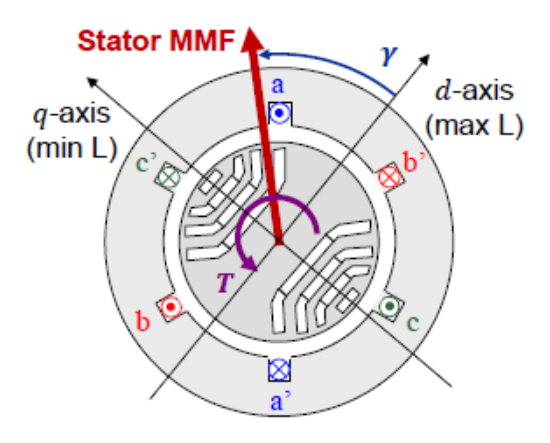


Figure 3.8. Geometry and torque generation of a SyRM

3.3.3 Permanent Magnet Synchronous Machine (PMSM)

In a typical permanent magnet synchronous machine (PMSM) the rotor excitation winding is replaced by permanent magnets, and the motor is driven by an electronic converter. This configuration is particularly common in medium to small-sized electric machines, typically up to several hundred kW. The magnetic flux generated by the PMs interacts

with the rotating field produced by the stator windings. Because the magnetic permeability of the magnets is close to that of air, the magnetic reluctance (and hence the inductance) remains nearly constant in all directions within the air gap. The torque production is the result of the rotor's tendency to align its magnetic axis (defined by the magnetic flux), with the stator magnetomotive force (MMF), thus producing the permanent magnet torque (PM torque). As for the case of SyRMs, precise control of the stator current components i_d , i_q is needed to ensure proper operation and torque optimization. A schematic representation of a typical PSMS is reported in Fig. 3.9.

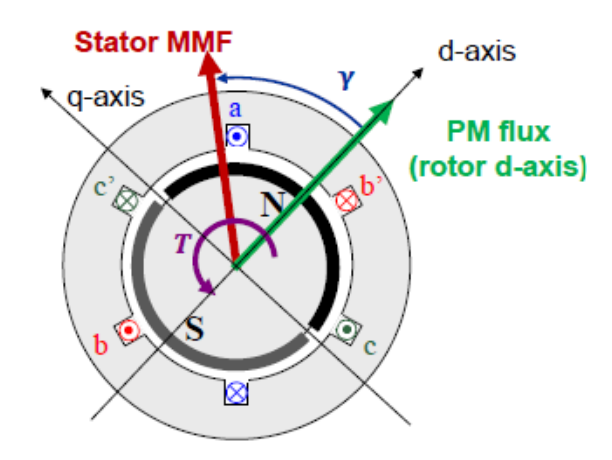


Figure 3.9. Geometry and torque generation of a PMSM

Different rotor configurations exits for PMSMs; the choice depends on the desired balance between torque density (PM and reluctance torque levels), structural robustness, and flux weakening capability.

3.3.4 SMs characteristics summary

To summarize, below is reported a table indicating all the most relevant ac machines configurations and relative characteristics:

	Asynchrono	ous motors	Synchronous motors				
	Squirrel cage	Wound rotor	SPM	IPM	PM-SyR	SyR	
Cost	Low	Low Medium-high Hig		Medium	Medium-low	Low	
Efficiency	Medium	Medium	High	High	High	Medium-high	
T density	Medium-high	Medium-high	Very high	High	Medium-high	Medium	
FW capability ^(*)	Medium-high	High	Very low(**)	Medium	Very high	Low	
Anisotropy	No	No	No	Low, $L_q > L_d$	High $L_d\gg L_q$	High $L_d \gg L_q$	
РМ	No	No (I		High (rare heart)	Low (rare hearth or ferrite)	No	
d axis	Rotor flux	Rotor flux	PM direction	PM direction	Max L	Max L	
Optimal γ	$0 < \gamma < \pi/2$	$0 < \gamma < \pi/2$	$\gamma = \pi/2$	$\pi/2 < \gamma < \pi$	$0 < \gamma < \pi/2$	$0 < \gamma < \pi/2$	

(*) FW = Flux Weakening, similar with Field Weakening for DC motor

Figure 3.10. Summary of motor types and characteristics [3]

3.3.5 WRSMs main applications

An extended literature review underscored that the wound rotor synchronous machine (WRSM) is a versatile EM that can be used both for generation, due to their ability to maintain synchronization, and motoring applications, due to precise speed and torque control.

Focusing on the latter, the main application fields are:

- **High-power applications**: industrial applications require precise speed control and high torque; the wound configuration allows for external control of the field current, enabling to satisfy these requirements by enabling a fine control over motor speed and torque. Typical applications are rolling mills, hoists, mines, and cement mills;
- Speed drive control: applications, such as conveyors or cranes, that require a demanding speed variability; WRSMs can guarantee a good performance curve across a wide speed range;
- Marine propulsion: WRSMs are particularly desired in heavy-duty marine applications due to their robustness, reliability, efficiency, and capability to generate high torque at low speed;
- Locomotives: although WRSMs has been widely used in this sector, in modern locomotives, almost all traction systems have shifted to Permanent Magnet Synchronous machines (PMSMs) or Induction motors (IMs), due to higher efficiency, better performances and lower maintenance costs;
- Reactive power compensation: by controlling the excitation of the rotor, WRSMs can regulate the power factor, allowing for supply reactive power to the grid.

^(**) Except concentrated winding machines

Chapter 4

Electrically Excited Synchronous Motor (EESM) in traction applications

4.1 Features of EESMs

As discussed in previous sections, "the Electrically Excited Synchronous Motor (EESM), is characterized by a highly optimized and refined architecture that ensures exceptional control accuracy and operational performance" [18]. The ability to dynamically regulate the excitation field and the advanced electromagnetic design make this type of motor very efficient, making it a viable alternative for the EV market.

In this motor, the stator armature windings are placed within laminated steel cores that are called slots. The design of the slots allows multiple parallel paths for the current, increasing the overall efficiency and reducing resistive losses. "To enhance space utilization while maintaining good fill factor and good insulation, stator has precise slot dimensions that enhances both the fill factor and good insulation" [19].

A distinctive feature of the EESM lies in its rotor construction; it employs field windings supplied by an external DC source through slip rings and brushes instead of permanent magnets (like PMSM); this allows, as fully discussed, direct control of the rotor flux and (consequently) of the electromagnetic torque. The resulting back electromotive force (EMF) is reduced, in turn reducing the voltage stator demand and, consequently, improving thermal stability and operational safety. To ensure uniform flux distribution across the air gap, structural components such as pole shoes and pole necks (incorporated in the rotor) are crucial. In some configurations, a permanent magnet can be included in the rotor to reinforce field stability and enhance magnetic performance.

The operation of the EESM depends on the interaction between the rotating magnetic field generated by the AC supply in the stator windings and the constant magnetic field produced in the rotor by the DC supply. The latter interaction causes the rotor to synchronize with the stator rotating magnetic field to synchronize, enabling the motor

to operate at a speed that is directly proportional to the frequency of the alternating current supply.

Efficient magnetic coupling and minimal losses can be achieved by carefully designing air-gap between stator and rotor. "Dynamic control of excitation current also offers significant benefits including optimizing torque production and operational efficiency over a wide speed range and loads" [20].

This controllable excitation makes the EESM remarkably versatile. By adjusting the rotor current, the motor can properly regulate the power factor and reactive power, ensuring precision and optimal energy conversion for various load conditions. Such flexibility, combined with its robust mechanical structure, makes the EESM particularly suitable for high-performance applications, which is the main focus of this work.

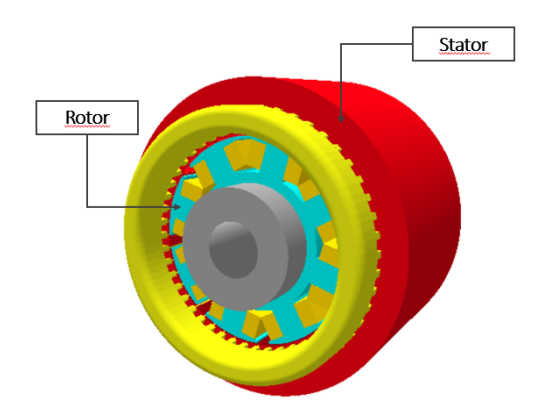


Figure 4.1. EESM wounded rotor structure (MotorCAD)

4.1.1 Advantages

The Electrically Excited Synchronous Motor (EESM) has several advantages:

- Rotor excitation: using rotor external excitation instead of permanent magnets (unlike PMSMs) the EESM allows for better magnetic flux control, and thus more flexibility in power management. Additionally, the EESM eliminates the need for rare-earth materials, thereby reducing reliance on these costly (and geopolitically) sensitive resources;
- High torque and wide speed range: the EESM can be optimized to deliver high torque at low speeds and during startup, thus improving, as a consequence, driving responsive in urban environments and efficiency across a wide range of speeds; the latter is particularly suitable for both city driving and highway cruising;
- Safety and advanced control: The EESM is capable of shutting down the field current in the event of converter failure at high speed thus improving safety; moreover, the ability to adjust the field current enables sophisticated control strategies, enhancing performance and efficiency;

• Adaptable power factor control: the excitation method allows to adapt the power factor, thus optimizing energy consumption for each driving condition, particularly in the field weakening ¹ operation range.

4.1.2 Disadvantages

Although the EESM offers a balance of performance, efficiency and sustainability, there are also some drawbacks:

- Complexity, size and weight: compared to PMSM technology, the EESM features a
 more complex design, due to the need of additional components such as excitation
 system, rings, bearings; these extra components not only compromise complexity
 but also result in larger and heavier motors, potentially impacting vehicle weight
 and available space for other components;
- Thermal management: the power consumed by the excitation system can also slightly reduce energy efficiency, particularly in low-load conditions, heating the rotor and consequently affecting the thermal performances (thus requiring a more complex and powerful thermal cooling design);
- Control control complexity and maintenance: EESMs require more maintenance than PMSMs, particularly due to components wear as for rings and brushes; furthermore, the ability to adjust the field current increases the control system complexity;
- Initial cost: the advanced technology and extra components required for EESMs lead to higher manufacturing costs compared to other technologies like PMSMs.

4.2 EESM in the automotive market

To follow the rapid growth of fully electric propulsion systems, EESM technology has emerged as a promising solution that offers high performance without the need of permanent magnets.

Following a literature review based mainly on *non-citable technical sources*, the currently available competitor solutions available on the market, compared with the technological approach adopted by *Stellantis*, are summarized and compared. The following overview therefore provides a purely illustrative and approximate benchmarking of the main e-motor configurations.

4.2.1 Renault ZOE

One of the earliest mainstream EVs to adopt WRSM technology. This version is equipped with e-front axle composed by a 4-pole EESM, a single-speed reducer, inverter, and oil

¹Field weakening is an electric motor control technique that allows the motor to exceed its rated speed by intentionally reducing its magnetic field

cooled system, that can produce approximately 65 kW of power and 220 Nm of torque. Rotor field excitation is proving with slip rings and brushes. The first generation model was equipped with a 22 kWh battery pack, achieving almost 240 km of range on the NEDS cycle.



Figure 4.2. Renault Zoe vehicle and EESM architecture [5]

4.2.2 Renault Megane E-tech

Built on the ZOE's architecture, the Renault Megane E-Tech adopts a 4-pole EESM that can deliver up to 160 kW and 300 Nm. The e-motor is integrated within a front e-axle that combines the inverter, a single-speed reducer, and oil-cooled system. In this case, two battery packs, respectively, of 22 and 40 kWh, are available on the market, both guaranteeing a minimum of 250 km of range.



Figure 4.3. Renault Megan vehicle and EESM architecture [6]

4.2.3 BMW - i4/iX Series

BMW is currently leading the adoption of EESM technology, particularly in its higher-end electric vehicles like the iX, a luxury electric SUV, the i4, an all electric Gran Coupe, and the iX3, the electric version of the X3 SUV [2].

Both i4 and iX models use a 6-pole EESM, excited by slip rings and brushes Excitation methods and with hairpin windings, that can deliver up to 400kW and nearly 800 Nm of torque in AWD configuration. Each axle employs a modular 3-1 unit (motor, inverter and gearbox integrated, as previous solutions), integrated with *hybrid oil-water* cooling.



Figure 4.4. BMW iX GenV powertrain

4.2.4 BYD Seal Excellence

Even if this model **does not use a EESM**, it is interesting to analyze different solutions on the market to further increase the quality of our benchmarket.

The BYD Seal Excellence is composed by a due-motor layout, combining a rear PMSM (rated at approximately $230~\rm kW$ and $360~\rm Nm$), and a front Asynchronous Motor ($160~\rm kW$ and $310~\rm Nm$). Both e-axles feature 3-1 oil-cooled solutions.



Figure 4.5. BYD Seal Excellence powertrain [7]

4.2.5 ZF

In 2023, at the Germany International Motor Show, ZF presented the I2SM (In-Rotor Inductive-Excited Synchronous Motor). Inductive rotor excitation, as discussed in previous sections, eliminates the need of permanent magnets, slip rings or brushes. ZF claims to have developed the world's most compact and highest torque density e-motor without the need of magnets or rare earth materials.

4.2.6 Comparative Overview

Model	Excitation Type	Conductor	$\mathbf{Q}\mathbf{s}$	Pole Pairs	P[kW]	T[Nm]
Renault Zoe	Brushes	Random	48	4	65	220
Renault Megane E-Tech	Brushes	Hairpin	-	4	160	300
BMW iX3	Brushes	Hairpin	54	6	400	800
BMW i4	Brushes	Hairpin	-	6	400	800
ZF I2SM	Inductive	Hairpin	36	6	-	=
BYD Seal Excellence	-	PMSM + Asynchronous	-	-	$230 \; (rear) + 160 \; (front)$	360 (rear) + 310 (front)

Table 4.1. Comparative technical data of EV with EESMs in the market

4.3 EESM design for high-speed and cost-effective for a Stellantis traction application

The purpose of this thesis work is to collaborate in the design phase of a high-speed and cost-effective EESM intended for a Stellantis application. Being still in a prototypal stage, the following chapter will purely describe the current state-of-art solutions for EESMs to provide an overview of the possible design directions that may be pursued according to initial EM imposed specifications reported in table below .

The design of a current-excited synchronous machine for the automotive field has to fuse three main objectives: high power density, cost efficiency, and reliability at very high rotational speeds. The target for the maximum speed is approximately 16000 rpm, with the objective of placing this motor in the same operational range as many PMSMs, may lead to various thermal and structural complications .

4.4 Rotor Pole Number

The number of poles directly affects both the electrical frequency and the mechanical stress of the rotor.

Considering the objective case, for high-speed applications, a low pole number, typically 4-8 poles, is generally preferred to limit electrical frequency, iron losses, and induced voltages in the field windings, affecting as a consequence the motor thermal stress. A higher number of poles of 10-12 is generally adopted for high-torque EESMs for heavy-duty vehicles, but increased frequency can lead to iron and copper losses.

Geometry	Value	Unit
Number of poles	8	_
Outer diameter	115.92	mm
Pole width	14.4	mm
Pole depth	15.5	mm
Pole tip width	11	mm
Pole tip depth	4.5	mm
Coil width	9	mm
Coil depth	14	mm
Maximum speed	16000	rpm
Base speed	4750	rpm
Current density	12	A/mm^2

Table 4.2. Initial data specifications for the EESM prototype.

An 8-pole configuration (4 pole pairs) represents a good compromise between dynamic performance and thermo-mechanical integrity, corresponding to a fundamental electrical frequency ² of about 317 Hz at rated speed (4750 rpm) and 1.07 kHz at maximum speed (16000 rpm).

4.5 Stator windings

To be cost- and space-oriented, with low AC losses, stator winding configuration has to be carefully chosen, as it strongly influences both the electromagnetic and thermal behavior of the motor.

Two stator windings technology are present in the market:

- **Distributed windings**: produce a nearly sinusoidal field distribution at the airgap; however, they have higher manufacturing cost and additional material (and so Joule losses);
- Concentrated windings are a cheaper solution but produce harmonic fields; for this reason, they are mainly used in fractional-HP, direct drive, and safety critical applications.

$$f = \frac{(p*n)}{120} \tag{4.1}$$

Where: p is the number of poles, n is the mechanical shaft speed

²The fundamental electrical frequency for synchronous machines is defined as

Two main types of conductor are commonly adopted in stator windings:

- Random (round) conductors: made of round wires randomly inserted within the slot; easy to manufacture, flexible solution and insulation strength but lower slot fill factor, limiting current and power density as a consequence;
- Rectangular (hairpin) conductors: use pre-formed rectangular copper bars blocked with pins within the slots; higher slot fill factor and better thermal conduction but, as opposite of the previous solution, manufacturing cost are higher and the solution is less flexible

In this prototype, the coil style is hairpin, arranged in an overlapping configuration with the impregnation liner material. Hairpin solution has been chosen, despite the higher cost, mainly for the excellent slot fill factors that reach, respectively, 0.85 in wire slot fill and 0.62 in copper slot fill.

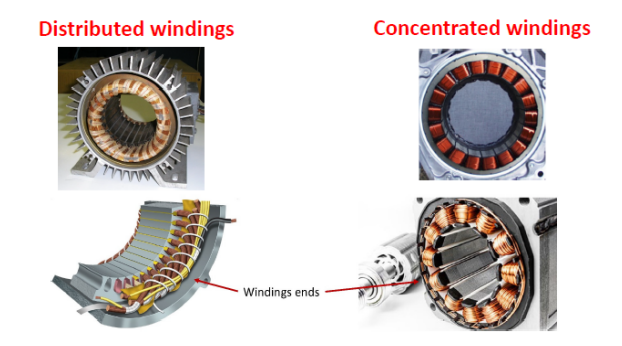


Figure 4.6. Distributed (left) and Concentrated (right) windings arrangement [3]

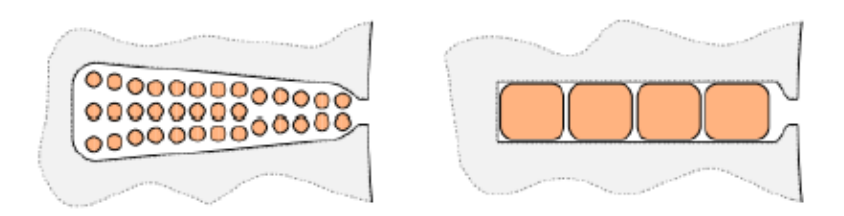


Figure 4.7. Copper conductors in random (left) and hairpin (right) winding [8]

4.6 Winding insulation

The insulation system must withstand both thermal cycling and partial discharge phenomena. The proposed solution employs a class H insulation system (180 C limit), enabling to maintain a compact design without excessive safety margins. Insulation clearances are also minimized in the air gap region, to minimize it up to 0.7 mm without risk

of dielectric breakdown (due to inverter spikes.

4.7 Supply System

The stator is powered by a conventional three-phase inverter field-oriented control (FOC), while the rotor excitation is supplied through a brushless exciter or rotating transformer, depending on the final implementation choice.

4.8 Cooling System

Cooling system strategies will be discussed in the next chapter. That said, at least in the prototype phase, it has been decided to employ a dual-circuit liquid cooling system, one for the stator and one for the rotor.

The stator will use a spiral water cooling jacket or a direct slot cooling solution, to maintain the temperature distribution uniform and below 150 C under all load conditions. The rotor instead, will use internal hollow conductors with coolant flowing through the stator.

The objective is to keep the temperature always below the imposed threshold also under continuous operation at 16 000 rpm. A generic configuration of this dual-circuit liquid cooling system is provided in the figure below (Audi E-Tron solution):

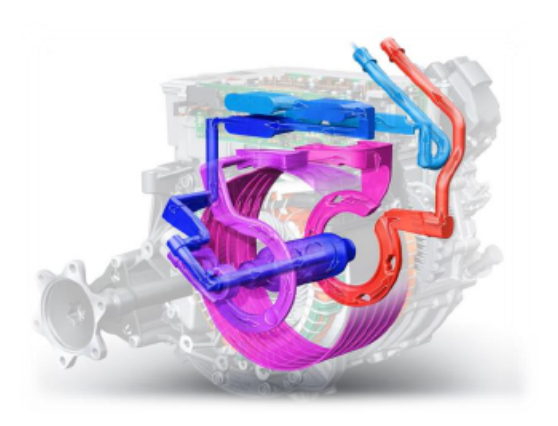


Figure 4.8. Audi e-tron cooling technology

Chapter 5

CFD: Computational Fluid Dynamics

Computational Fluid Dynamics (CFD) has now become an indispensable tool in almost all fields of engineering, as it accelerates and reduces development costs, enables the creation of highly optimized designs and facilitates processes that are difficult to examine experimentally. However, computational resources plays a central role in this field, particularly in optimization processes, where hundreds of simulation cycles are required.

Incompressible flows are a very important subclass of CFD, and are precisely the focus of the present thesis work. A 50/50 EGW-oil solution, which is a solution that mixes equal parts of ethylene glycol-water and oil, will be used as a coolant.

The main purpose of CFD is to solve the Navier-Stokes equations (NSE) and all the constraint equations related to them. The analytical resolution of these equations is feasible only for a very limited number of cases with laminar flows and very simple geometries. For turbulent flows, with highly complex geometries and boundary conditions involved, numerical resolution becomes practically mandatory.

The current main computational fluid dynamics techniques, such as the Finite Volume Method (FVM) or the Finite Difference Method (FDM), attempt to solve the conservation equations of mass, momentum, and energy over a finite number of nodes or volumes into which the flow field is divided. Therefore, they are methods based on the continuum hypothesis, that is, on a macroscopic description of the flow.

5.1 CFD generic structure

Generally, a CFD simulation consists of the following phases:

- **Problem formulation**: in this initial phase, the objectives of the analysis, the operating conditions, and the adopted time model (steady or unsteady) are defined;
- Geometry and computational domain: by using a CAD software, the geometry of the body is defined; all the finite regions in which the simulation will take place

are "enclosed" in regions called computational domains. Its always advisable to prepare models with the simplest possible geometries to avoid excessive computational effort;

- Mesh generation: the domain is divided into (millions of) small volumes within which the governing equations are locally solved. The quality of the simulation strictly increased with the accuracy of the mesh, but increasing the computational cost as a consequence;
- Selection of the optimal solving algorithm
- Assignment of the physical properties and boundary conditions: boundary conditions, initial values of all the field variables (velocity, density, pressure, etc.) are specified; an iterative process on which the solution of the governing equation is based will start (Initialization);
- Simulation: conservation equations are solved iteratively at the center of each cell and the process proceeds until convergence to the final solution is reached (although it may also diverge, resulting in no solution). In this work, a residual convergence error of 10⁻⁶ is imposed for the momentum equation and 10⁻⁸ for the energy equations to ensure a reliable solution without increasing too much the computational effort;
- **Post-processing**: obtained data are analyzed through graphical visualization of the most significant flow field variables (in this case pressure, temperature, and total heat transfer).

5.2 Governing equations

The goal of CFD is to solve the equations governing the motion of fluid, known as the continuity equation and the Navier-Stokes equations (NSE). In the incompressible case, these equations form a closed system of partial differential equations whose unknowns are the pressure p and the three velocity components u, v, w.

5.2.1 Reynolds Transport Theorem (RTT)

A macroscopic property is called *intensive* when it does not depend on the mass of the system; it is called *extensive* when it explicitly depends on mass. The intensive property η is the corresponding extensive property N per unit mass. Conservation laws are often written for a moving mass of fluid (Lagrangian or material description), while in CFD we refer to a *fixed* control volume (Eulerian or spatial description). For a generic property η of the flow, The *Reynolds Transport Theorem* (*RTT*) allows the connection between the two descriptions:

$$\frac{dN}{dt} = \frac{\partial}{\partial t} \int_{CV} \rho \, \eta \, dV + \int_{CS} \rho \, \eta \, (\mathbf{u} \cdot \mathbf{n}) \, dA$$
 (5.1)

where: N is the extensive property; η the corresponding intensive property; ρ density; \mathbf{u} velocity vector; CV the control volume; CS its control surface; \mathbf{n} the outward unit normal.

5.2.2 Mass Conservation (Continuity equation)

The conservation of mass for any fluid mass M states

$$\frac{dM}{dt} = 0\tag{5.2}$$

where: M is the total mass of the system.

With N=M and $\eta=1$ in Eq. (5.1), the integral continuity equation for a fixed CV is

$$0 = \int_{CV} \frac{\partial \rho}{\partial t} dV + \int_{CS} \rho \left(\mathbf{u} \cdot \mathbf{n} \right) dA$$
 (5.3)

where: $\partial \rho / \partial t$ is the local (unsteady) density variation; $\rho(\mathbf{u} \cdot \mathbf{n})$ is the mass flux through CS.

Using the divergence theorem,

$$\int_{CV} \left(\frac{\partial \rho}{\partial t} + \nabla \cdot (\rho \mathbf{u}) \right) dV = 0$$
 (5.4)

where: $\nabla \cdot (\rho \mathbf{u})$ is the divergence of mass flux.

Since CV is arbitrary,

$$\frac{\partial \rho}{\partial t} + \nabla \cdot (\rho \mathbf{u}) = 0 \tag{5.5}$$

where: Eq. (5.5) is the differential continuity equation.

For incompressible flow $(\partial \rho/\partial t = 0 \text{ and } \rho = \text{const})$,

$$\nabla \cdot \mathbf{u} = 0 \tag{5.6}$$

This condition enforces the volume conservation (i.e, no volumetric dilation).

5.2.3 Momentum Conservation (NSE)

The conservation of linear momentum for a fluid is:

$$\frac{d\mathbf{q}}{dt} = \mathbf{B} + \mathbf{F} \tag{5.7}$$

where: \mathbf{q} is total momentum; \mathbf{B} is the resultant of body forces (e.g. gravity), and \mathbf{F} of surface forces (pressure and viscous stresses).

For a fixed control volume, applying RTT to the momentum equation $(N = m\mathbf{u}, \eta = \mathbf{u})$,

$$\frac{d}{dt} \int_{CV} \rho \,\mathbf{u} \,dV + \int_{CS} \rho \,\mathbf{u}(\mathbf{u} \cdot \mathbf{n}) \,dA = \int_{CV} \rho \,\mathbf{g} \,dV + \int_{CS} [\sigma_{ij}] \cdot \mathbf{n} \,dA \qquad (5.8)$$

where: **g** is gravitational acceleration; $[\sigma_{ij}]$ is the Cauchy stress tensor (pressure + viscous stresses).

Using the divergence theorem and the arbitrariness of CV:

$$\frac{\partial(\rho \mathbf{u})}{\partial t} + \nabla \cdot (\rho \mathbf{u} \otimes \mathbf{u}) = -\nabla p + \nabla \cdot [\hat{\tau}_{ij}] + \rho \mathbf{g}$$
 (5.9)

where: $\rho \mathbf{u} \otimes \mathbf{u}$ is the tensor of convective momentum flux; $-\nabla p$ represents the pressure gradient; $\nabla \cdot [\hat{\tau}_{ij}]$ is the divergence of viscous stresses; $\rho \mathbf{g}$ is the body force per unit volume (e.g., gravity).

The total stress tensor $[\sigma_{ij}]$ is split into pressure and viscous parts:

$$[\sigma_{ij}] = -p[I_{ij}] + [\hat{\tau}_{ij}] \tag{5.10}$$

where: $[I_{ij}]$ is the identity tensor; $[\hat{\tau}_{ij}]$ is the viscous stress tensor.

For a Newtonian, isotropic, and isothermal fluid, viscous stresses are linearly proportional to the strain rate tensor:

$$[\hat{\tau}_{ij}] = 2\mu[\epsilon_{ij}] \tag{5.11}$$

where: μ is the dynamic viscosity; $[\epsilon_{ij}]$ is the symmetric rate-of-strain tensor defined as

$$[\epsilon_{ij}] = \frac{1}{2} \left(\nabla \mathbf{u} + \nabla \mathbf{u}^{\mathrm{T}} \right).$$

Substituting Eq.(5.11) into Eq.(5.9) and dividing by ρ , yields the compact vector form of the Navier-Stokes equations:

$$\frac{\partial \mathbf{u}}{\partial t} + (\mathbf{u} \cdot \nabla)\mathbf{u} = \mathbf{g} - \frac{1}{\rho} \nabla p + \nu \nabla^2 \mathbf{u}$$
 (5.12)

where: $\nu = \mu/\rho$ is the kinematic viscosity; $(\mathbf{u} \cdot \nabla)\mathbf{u}$ is the convective acceleration; $\nabla^2 \mathbf{u}$ is the viscous diffusion of momentum.

Coupled with Eq. (5.6), Eq. (5.12) and (5.6) form the incompressible Navier - Stokes system:

$$\begin{cases} \nabla \cdot \mathbf{u} = 0, \\ \frac{\partial \mathbf{u}}{\partial t} + (\mathbf{u} \cdot \nabla)\mathbf{u} = \mathbf{g} - \frac{1}{\rho} \nabla p + \nu \nabla^2 \mathbf{u}. \end{cases}$$
 (5.13)

where: the four unknowns are p, u, v, w; analytical solutions exist only for a few simple laminar configurations, so numerical CFD solvers are generally required.

5.2.4 Energy Conservation Equation

The first law of thermodynamics (energy conservation) for a continuum can be written in conservative form as:

$$\frac{\partial(\rho E)}{\partial t} + \nabla \cdot (\rho E \mathbf{u}) = -\nabla \cdot (p\mathbf{u}) + \nabla \cdot ([\hat{\tau}_{ij}] \mathbf{u}) - \nabla \cdot \mathbf{q} + \rho \mathbf{u} \cdot \mathbf{g} + \dot{q}_v \quad (5.14)$$

where: $E = e + \frac{1}{2} |\mathbf{u}|^2$ is the specific total energy; $-\nabla \cdot (p\mathbf{u})$ is the work done by pressure forces; $\nabla \cdot ([\hat{\tau}_{ij}]\mathbf{u})$ is the power of the viscous tensor; \mathbf{q} is the heat flux according to

Fourier's law; $(\rho \mathbf{u} \cdot \mathbf{g})$ is the power of body forces; \dot{q}_v is a volumetric heat source (e.g., radiation, Joule effect).

Alternatively, in internal energy form:

$$\rho \frac{De}{Dt} = -p \nabla \cdot \mathbf{u} + [\hat{\tau}_{ij}] \nabla \cdot \mathbf{u} - \nabla \cdot \mathbf{q} + \dot{q}_v$$
 (5.15)

where: De/Dt is the material derivative of the internal energy; $-p\nabla \cdot \mathbf{u}$ is the work of compression/expansion; $[\hat{\tau}_{ij}]\nabla \cdot \mathbf{u}$ is the viscous dissipation Φ ; $-\nabla \cdot \mathbf{q}$ is thermal conduction; \dot{q}_v represents volumetric heat generation.

Using $e = c_v T$ and $\mathbf{q} = -k \nabla T$, for a Newtonian with constant fluid property:

$$\rho c_v \frac{DT}{Dt} = -p \nabla \cdot \mathbf{u} + \Phi + \nabla \cdot (k \nabla T) + \dot{q}_v$$
 (5.16)

where: T is temperature; c_v specific heat at constant volume; k thermal conductivity; Φ viscous dissipation term.

For incompressible flow $(\nabla \cdot \mathbf{u} = 0)$ and constant properties:

$$\rho c_p \left(\frac{\partial T}{\partial t} + \mathbf{u} \cdot \nabla T \right) = \nabla \cdot (k \nabla T) + \Phi + \dot{q}_v$$
 (5.17)

where: c_p is the specific heat at constant pressure ($c_p \simeq c_v$ for liquids); LHS represents the transient and convective transport of thermal energy; RHS represents conduction, viscous heating, and volumetric sources.

5.2.5 Coupling of the equations

Equations (5.5), (5.12), and (5.17) represent the complete set of governing equations for a Newtonian, incompressible, and thermally conducting fluid:

$$\begin{cases} \nabla \cdot \mathbf{u} = 0, \\ \frac{\partial \mathbf{u}}{\partial t} + (\mathbf{u} \cdot \nabla)\mathbf{u} = \mathbf{g} - \frac{1}{\rho} \nabla p + \nu \nabla^2 \mathbf{u}, \\ \rho c_p \left(\frac{\partial T}{\partial t} + \mathbf{u} \cdot \nabla T \right) = \nabla \cdot (k \nabla T) + \Phi + \dot{q}_v. \end{cases}$$
(5.18)

These three equations express, respectively, conservation of mass, momentum, and energy, and by joining them together it is possible to obtain the fundamental mathematical model that governs fluid dynamics.

5.3 Governing equations solving methods

The main methods for solving the Navier-Stokes equations are:

• Direct Numerical Simulation (DNS): method that assigns time-dependent fluctuating velocity components as boundary conditions, allowing to solve unsteady turbulent flows (so unsteady NSE) over all spatial and temporal scales. This method is highly accurate but extremely computationally expensive, thus it can be used only for studying locally turbulent flows;

- Reynolds Averaged Navier-Stokes (RANS): in this case the turbulent motion can be decomposed into two components (to simplify the calculation): mean component and time-dependent fluctuation. The governing equations are therefore decomposed and time-averaged and this, performed over a certain time-step, gives birth to the Reynolds Averaged Navier-Stokes. This is the most widely used approach for engineering applications as it significantly reduces the computational cost;
- Large Eddy Simulation (LES): employs specific numerical filters to separate and remodel the turbulence scales. The large flow scales are solved directly, while the smaller scales are modeled. This method is more accurate than RANS and less computationally demanding than DNS, which is why it is currently under rapid development.

5.4 Heat transfer

5.5 Heat transfer models

"Heat transfer is thermal energy in transit due to a partial temperature difference" [9]. Whenever a temperature difference exists in a medium, heat transfer must occur; this transfer can happen in three main mechanisms:

- Conduction: heat transfer that occurs across a medium that can be solid or fluid, in presence of a temperature difference;
- Convection: heat transfer occurs between a surface and a moving medium when there is a delta difference between them;
- Radiation: "All surfaces of finite temperature emit energy in the form of electromagnetic waves. Hence, in the absence of an intervening medium, there is not heat transfer by radiation between two surfaces at different temperatures" [2].

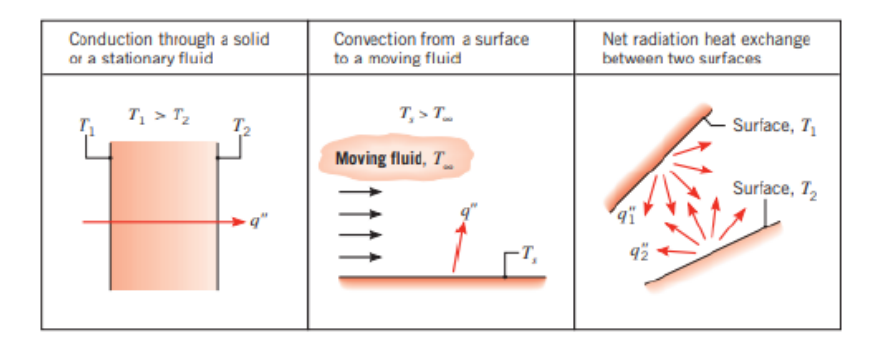


Figure 4.1: Conduction, convection and radiation [34]

Figure 5.1. Three main heat transfer mechanisms: conduction, convection, and radiation [9]

In this chapter, the fundamental physical principles, among with the governing rate equations of these heat transfer mechanisms are outlined.

Conduction and convection usually represent the predominant heat transfer mechanisms in electrical machines (i.e, the most efficient methods for managing thermal energy); radiative heat transfer, especially in our study case, contribute to a lesser extent and can be considered negligible.

5.5.1 Conduction

Heat conduction occurs primarily through two distinct mechanisms: molecular interaction and the motion of free electrons.

In the first case (microscopic mechanism), thermal energy is transferred by *lattice vibrations*, as molecules at higher temperature, that possess greater kinetic energy, continuously interact (collide) with molecules of lower energy, thereby transferring heat. This process occurs in solids, liquids, and gasses, and always follows the *second law of ther-modynamics*, which states that heat flows spontaneously from regions of higher to lower temperature.

The second mechanism (macroscopic) is due to the *transport of free electrons* between the medium; this mechanism is predominant in pure metals and in some liquids. Metal alloys have a variable number of free electrons, thus they exhibit a lower thermal conductivity; non-metallic materials instead, which possess very few mobile charge carriers, are poor conductors. Consequently, the ability of a solid to conduct heat depends largely on the concentration and mobility of free electrons within the material. That is why pure metals are generally the most efficient thermal conductors.

Conduction heat transfer rate The rate of conductive heat transfer is expressed by Fourierâs law; considering a one-dimensional temperature distribution T(x), this law can be written as follows:

$$q_x'' = -k \frac{dT}{dx} \quad [W/m^2] \tag{5.19}$$

where: q_x'' is the heat flux (heat transfer rate per unit area) in the x-direction. The area is intended normal to the direction of heat flow; k is the thermal conductivity of the material [W/(m K)]; and $\frac{dT}{dx}$ is the local temperature gradient.

The negative sign indicates that heat is transferred in the direction of decreasing temperature. The *thermal conductivity* k is a thermo-physic parameter that quantifies the ability of the medium to transmit heat.

The total rate of heat transfer through a plane wall of cross-sectional area A is therefore obtained by multiplying it with Eq. 5.19:

$$q_x = -k A \frac{dT}{dx} \quad [W] \tag{5.20}$$

where: q_x represents the overall conductive heat transfer rate across the plane.

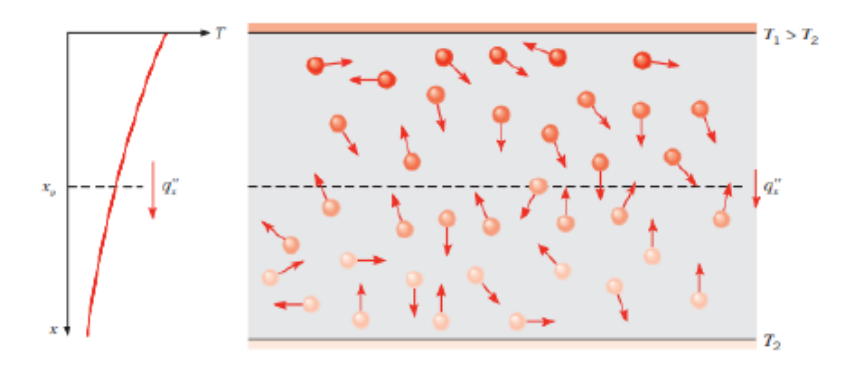


Figure 5.2. Conduction energy transfer mechanism [9]

5.5.2 Convection

Convection takes place between a solid surface and a fluid in motion and it involves two mechanisms: energy exchange by *molecular diffusion*, resulting from random molecular motion, and energy transport by the *bulk movement* of the fluid, known as *advection*. The convection process generally refers to this combined effect and it takes place only when a temperature difference exists between the surface and the fluid.

Boundary layers When a fluid flows over a surface maintained at a temperature different from that of the flow, two layers develop: the velocity boundary layer, where the fluid velocity increases from zero at the wall to a free-stream value u_{∞} , and the thermal boundary layer, where temperature varies from the surface temperature T_s at y=0 to the free-stream temperature T_{∞} . The relative thicknesses of these two layers depend on the fluid properties and the flow regime. If $T_s > T_{\infty}$, heat is transferred from the wall to the fluid; when $T_s < T_{\infty}$, the direction is reversed. Close to the wall, where the velocity approaches zero, the conduction process dominates; farther away instead, convective transport becomes prevalent as thermal energy is carried by the flow.

Flow regime Depending on the velocity field within the boundary layer, heat transfer can be strongly influenced. Three main regimes can be identified:

- Laminar flow: the motion of the fluid is typically smooth and ordered and adjacent fluid layers slide over one another regularly. The velocity gradient is gradual, and the flow remains stable;
- Transitional flow: occurs between laminar and turbulent regimes, due to small instabilities that grow within the boundary layer;
- **Turbulent flow:** at higher velocities or over rough surfaces, the motion becomes irregular and chaotic, producing intense mixing of fluid particles across the layer. This regime is characterized by thicker boundary layers, stronger momentum and heat transfer, and greater energy dissipation.

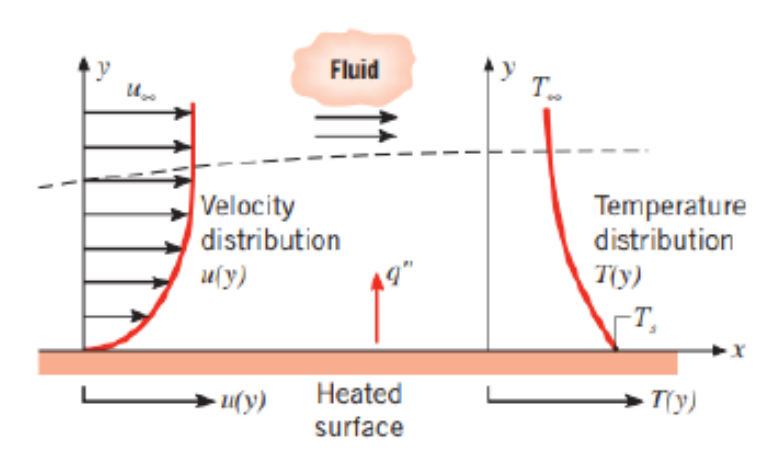


Figure 5.3. Boundary layer development in the convection heat transfer [9]

Convective heat transfer rate It is important to say that convection can be classified as forced or natural depending on the flow's driving mechanism. In forced convection, the motion is generated by external drivers (e.g. fans or pumps), and the heat transfer depend almost exclusively on flow conditions, while in natural convection, the motion results from buoyancy forces due to temperature-induced density differences.

Regardless of the flow regime and convection type, the local convective heat flux is expressed by the *Newton's cooling law*:

$$q'' = h (T_s - T_{\infty}) \quad [W/m^2]$$
 (5.21)

where: q'' is the convective heat flux normal to the surface; h is the convective heat transfer coefficient [W/(m² K)]; T_s and T_∞ are, respectively, the surface and free-stream fluid temperatures.

A positive q'' indicates heat transfer from the surface to the fluid $(T_s > T_\infty)$, while a negative value indicates the opposite situation $(T_s < T_\infty)$.

By multiplying the previous equation by a surface of area A, we obtain the total convective heat transfer rate over that surface:

$$q = h A (T_s - T_{\infty}) \quad [W] \tag{5.22}$$

where: q is the overall heat transfer rate between the surface and the fluid; A is the exposed surface.

It is worth to mention that, as in the conduction case, the value of q is the same for both fluid and wall that are exchanging heat,

For internal flows, the bulk or mean fluid temperature T_m replaces T_{∞} , playing an equivalent role to the free-stream temperature in external convection:

$$q = h A \left(T_s - T_m \right) \tag{5.23}$$

where: T_m is the mass-averaged fluid temperature, and plays the same role as the free-stream temperature for external flows.

The convective heat transfer coefficient h $[W/m^2K]$ depends on the boundary layer (e.g surface geometry) and on the nature of fluid motion and its properties. For engineering purposes, these coefficients are almost exclusively determined from experimental correlation and using three dimensionless number: Reynolds number (Re)¹, Prandtl number (Pr)², and Nusselt Number (Nu)³.

Process	$\frac{h}{(W/m^2 \cdot K)}$
Free convection	
Gases	2-25
Liquids	50-1000
Forced convection	
Gases	25-250
Liquids	100-20,000
Convection with phase change	
Boiling or condensation	2500-100,000

Figure 5.4. Convection heat transfer coefficient h typical values [9]

5.5.3 Radiation

When energy is transferred by electromagnetic waves, the heat transfer involved is radiation. This energy transfer does not require any medium and can consequently occur even through a vacuum.

"Every object with a temperature above absolute zero emits thermal radiation due to changes in the electron configurations of its atoms or molecules" [9].

$$Re = \frac{\rho vL}{\mu} = \frac{vL}{\nu}$$

where ρ : fluid density [kg/m³], v: velocity [m/s], L: characteristic length [m], μ : dynamic viscosity [Pa*s], and $\nu = \mu/\rho$: kinematic viscosity [m²/s]

$$Pr = \frac{c_p \mu}{k}$$

where c_p : specific heat at constant pressure [J/kg*K], μ : dynamic viscosity [Pa*s], and k: thermal conductivity [W/m*K]

³Ratio of convection heat transfer to conduction heat transfer over a representative thickness

$$Nu = \frac{hL}{k}$$

where h: convective heat transfer coefficient [W/m²*K], L: characteristic length [m], and k: thermal conductivity [W/m*K]

¹Compare the inertial forces to viscous forces and it helps characterizing flow condition: laminar, turbulent, or transition.

 $^{^2}$ Ratio of momentum diffusivity to thermal diffusivity; useful to compare the thermal boundary layer thickness with bounday layer viscosity.

A blackbody is defined as an ideal surface that absorbs and emits all radiation at every wavelength. The emissive power of a blackbody is defined by the *Stefan-Boltzmann law*:

$$E_b = \sigma T_s^4 \tag{5.24}$$

where T_s is the absolute temperature of the surface [K], and σ is the Stefan–Boltzmann constant.

Real surfaces emit less energy than a blackbody; an *emissivity coefficient* ϵ is added to the previous formula to characterize this effect; this coefficient ranges from 0 to 1 and quantifies how efficiently the surface emits compared to the ideal case:

$$E = \varepsilon \sigma T_s^4 \tag{5.25}$$

"Radiation may also be incident on a surface from a source in its surroundings. When radiation meets an object, part of it is absorbed into the object, some is reflected back from the surface of the object and some may transmit through the object" [2].

The rate of this absorption per unit area is determined by the absorptivity α :

$$G_{\rm abs} = \alpha G \tag{5.26}$$

Opaque surfaces have $\alpha < 1$ and thus part of the irradiation is reflected, whereas semi-transparent materials can also transmit a fraction of it.

When radiation exchange occurs between a small surface and a surface large enough to be considered isothermal (at T_{sur}), the irradiation can then be approximated as blackbody emission from the surroundings:

$$G = \sigma T_{\text{sur}}^4 \tag{5.27}$$

Under this condition, the net radiative heat flux from the surface is:

$$q_{\rm rad}^{"} = \varepsilon \sigma \left(T_s^4 - T_{\rm sur}^4 \right) \tag{5.28}$$

This equation represents the balance between the energy emitted by the surface and that absorbed from the surroundings.

For engineering purposes, this relation can be linearized; to achieve this condition, it is possible to define an equivalent radiation heat transfer coefficient h_r , so that the heat rate becomes proportional to a simple temperature difference:

$$q_{\rm rad} = h_r A (T_s - T_{\rm sur}) \tag{5.29}$$

where

$$h_r = \varepsilon \sigma (T_s + T_{\text{sur}})(T_s^2 + T_{\text{sur}}^2)$$
(5.30)

This form allows radiation to be treated as convection for thermal network models.

It is relevant to underline that, unlike the convective heat transfer coefficient h, the radiative coefficient h_r strongly depends on temperature, thus radiation increases significantly for surfaces with high temperature.

Chapter 6

Stator Cooling systems for high speed and torque/density motors

In recent years, compact electric machines with high torque and power density have become the focal point of the automotive industry. The purpose is to improve drivetrain integration, but it can often lead to higher current densities and/or rotor speeds, which can turn increase losses and thermal stress on the motor.

Consequently, effective cooling strategies are essential to ensure motor reliability and performance in each operating condition.

"While operating an electric motor, heat is generated due to the electromagnetic losses, mechanical power losses, and other stray losses that take place in various components within an electric motor. Through conduction, convection, and/or radiation, the thermal energy is transferred to a cooling medium on the basis of a temperature difference between the hot and cold bodies [21]".

Excessively high temperatures can lead to both insulation and winding conductors aging phonemena; thus, a correct motor thermal management is essential, especially during critical operating conditions, such as overload, and/or symmetric faults, to avoid failures usually due to local hot spot and material degradation.

6.1 Stator Cooling Methods

An overview of the state-of-art in electric motor cooling technologies is provided in the following chapter. The aim is to identify and analyze the most effective method for improving the competitiveness of the prototype while maintaining the same torque/power density.

In this work, the goal is not to further increase the power density of the machine, but to maintain a high level of performance while reducing overall system costs. To achieve this purpose, the most effective stator cooling solution is found under comparable operating conditions. Accordingly, the analysis conducted in this work focuses on keeping the overall stator maximum temperature below a certain threshold, to ensure reliable operation and thermal stability.

Based on the cooling method, we can distinguish between:

- **Natural passive cooling**: where heat is dissipated using on-site energy combined with the configuration of motor components;
- Forced cooling: where heat is dissipated by an external device and source of energy. The aim is to create sufficient coolant flow to exchange and extract heat from hotter components. Depending on the coolant nature, this method can be further divided in:
 - Forced Gas Cooling
 - Forced Liquid Cooling

the table below provides a comparative overview of the main cooling methods currently available on the market:

Cooling method		σ, kPa	A_l , kA/m	J, A/mm ²	h, W/m ² K
Natural convection		-	-	1.5-5	5-30
Forced	Air	<15	<80	5-10	20-300
gas cooled	Hydrogen	<25	70-110	7-12	100–1000
Forced	Indirect	20-60	90-130	7-20	100-10000
liquid cooled	Direct	60-100	100-200	10-30	200-25000
	Phase change	-	-	-	500-50000

Figure 6.1. Typical data for different cooling strategies [10]

Another classification can be done considering the component from which heat is extracted:

- · Housing cooling
- Stator-core cooling
- Winding cooling
- Rotor cooling

The present work aims to implement an effective (finding the most cost competitive solution) stator cooling strategy thus, this chapter will only analyze the current stator cooling technologies as discussed in [11], [22], [23], and [2].

6.2 Natural passive cooling

This method employs the housing as the primary heat exchanger component; energy is transferred by convection heat dissipation from the internal components to the surrounding environment. Therefore, optimizing the housing design is crucial to maximize the dissipation rate.

To achieve that, cooling fins (axial or radial) are normally placed on the external surface of the housing; key design objective is to maximize heat rate while minimizing cooling fin weight and volume. This approach is valid only on low-medium-power solutions, as the heat rate is usually not sufficient and is strongly dependent on ambient conditions. A common practice to improve heat dissipation is to extend the fin area and other parameters (figure below), although this increases air flow resistance, consequently decreasing the gain factor.

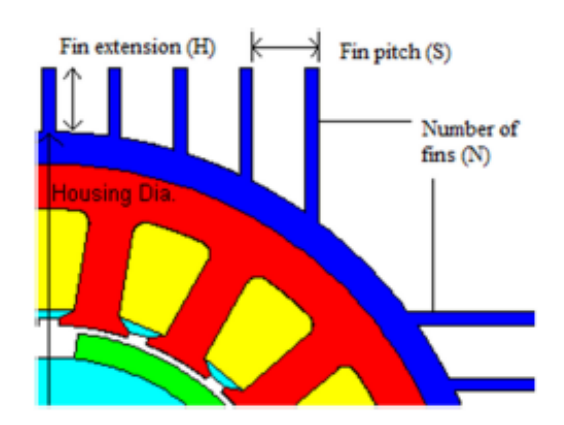


Figure 6.2. Natural Passive Cooling - fin configuration geometry [11]

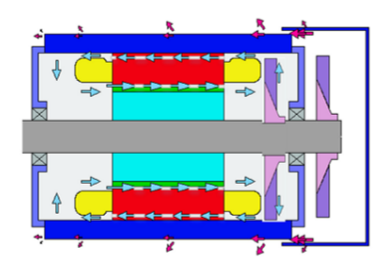
6.3 Forced gas cooling

Forced cooling is generically the most popular approach as it allows for more compact and power designs. In this situation, Reynold number (Re), discussed in previous section, is a crucial parameter as it allows to determine flow regime under different cooling media and architectures.

Two different varieties are available on the market: an enclosed fan cooled (EFC) motor, and an open fan cooled (OFC) motor.

An EFC motor uses a closed internal air circuit, which means that an internal fan recirculates air by transferring the heat from the motor to the housing; the latter is then externally cooled by air or air-to-water exchanger. In this design, "the motor is completely housed in a sealed enclosure that prevents dust and other contaminants from entering and affecting the internal components [2]".

In an OFC motor instead, air is not recirculated, as it is drawn from the ambient environment into the motor enclosure. For this reason, additional filters or indirect channels are required to prevent dust and moisture contamination.



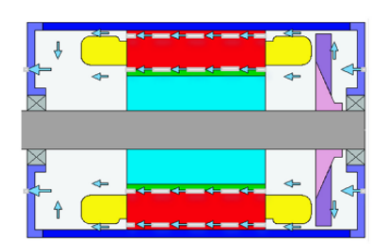


Figure 6.3. Ventilation on EFC (left) and OFC (right) motor

In such fan-based cooling systems, aerodynamic design of the blades is crucial, as the fan is responsible for the pressure difference needed to drive airflow through the motor; thus, a bad optimization of blade geometry and angle of attack can lead to higher energy losses and consequently heat transfer efficiency degradation.

6.4 Forced liquid cooling

Forced-liquid cooling systems are particularly suitable for high-power electric motors, overcoming the insufficient thermal requirements that forced gas cooling systems cannot satisfy.

In this configuration, the coolant is circulated throw channels in the housing, stator and/or rotor, and it transfers efficiently the heat away from internal components. Water is mainly used as a coolant fluid, although ethylene glycol-water oil mixtures (EGW 50/50) are becoming interesting solutions for commercial applications.

These cooling methods are particularly interesting for their effectiveness, although they have drawbacks such as corrosion, leakage, contamination, and deposits that can increase flow resistance and reduce overall cooling performance

6.4.1 Housing Water Jacket Cooling

This method represents the most common forced-cooling approach. In the housing jacket in fact, "the liquid flows through the cooling channels situated in a thermally conductive frame above the stator stack [24]".

The heat produced in the motor components such as coils, stator and rotor lamination, is removed from the housing by convection through the circulating coolant. The overall efficiency is strictly dependent on the thermal contact between the stator core and the housing, as poor contact can significantly increase the windings temperature, leading to structural and thermal problems.

Despite the cost-competitiveness, the main drawback of the solution lies in the fact that, while the liquid jacket is particularly efficient for the stator active stator parts, it is also less efficient in dissipating heat from more internal parts, such as end windings and the rotor, due to the greater thermal resistance between these regions and the coolant. To enhance thermal dissipation, different configurations and alternative coolants, such as gearbox lubricating oils, can be used.



Figure 6.4. Housing Water Jacket cooling solutions: zigzag (left) and spiral (right) [12]

6.4.2 Direct Slot Cooling

This liquid cooling method implies cooling via axial ducts within the stator yoke or the winding slots. To achieve this configuration, a sleeve in the rotor-stator gap is used to physically separate the two components and to prevent oil from entering in this gap, avoiding excessive windage losses. The coolant can be used only for the stator or taken from the stator cooling by dual-channel cooling configuration.

Although this solution is mainly suitable for high-speed PMSMs, as most of the loss is generated in the stator, direct slot cooling is starting to expand into EESMs, because of the increase of high-performance requirements in critical operations.

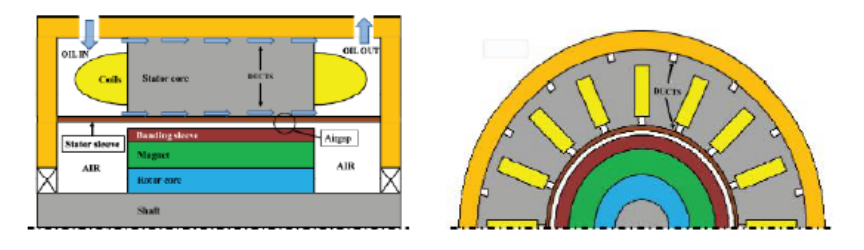


Figure 6.5. Direct Slot Cooling with sleeve and axial ducts [13]

6.4.3 Oil-flooded Cooling

Oil-flooded cooling systems enable for direct interaction between the coolant and the entire stator. It is generally a more efficient cooling method as the oil directly surrounds

the stator, increasing the heat removal; oil leakage and pressure drops are then the main concerns of this configuration.

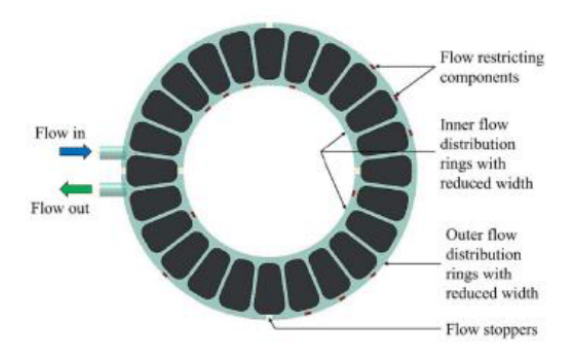


Figure 6.6. Oil-flooded stator of an axial-flux motor [14]

6.4.4 End-tip Cooling

Hot spots appear mainly at the end of the windings, as they represent a significant heat source and generally have a poor thermal insulating coating. To address this problem, some cooling techniques focus on heat extraction directly from the windings. Different strategies, such as cooling channel and potting materials, can be adopted.

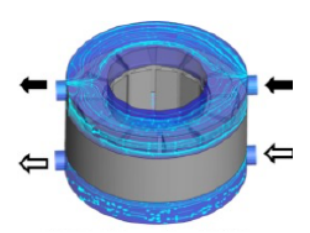


Figure 6.7. End-tip cooling method schematic

6.4.5 Oil-spray Cooling

This is a phase change cooling system where the coolant enters the system in liquid form, is pumped into the heat source, and it evaporates.

The evaporation is the consequence of the heat extraction; the gas is then recirculated back into the compressor before being returned to the liquid state, and the cycle starts again. This method is particularly efficient at dissipating heat and requires a smaller working volume than the previous solutions.

As the name suggests, oil spray cooling involves oil as a cold dielectric fluid. Oil can in fact guaranty huge energy transfers because of its large latent heat of evaporation and can maintain a uniform winding temperature across all the operational range.

Unlike previous cooling solutions, oil spray is less complex and does not require the motor to be sealed with a sleeve. Despite all these key characteristics, this method does not achieve the same level of uniform heat removal as, for example, oil-flooded cooling, which maintains a better heat distribution.

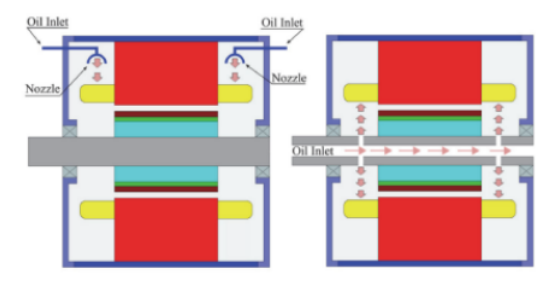


Figure 6.8. Oil spray cooling in different configurations: nozzle on top of the end-winding (left) and through the hollow shaft (right) [15]

Chapter 7

EESM prototype design (MotorCAD)

Based on the initial specification provided in Tab. 4.2 the main geometry dimensions and parameters, both for the stator and rotor, have been retrieved and set up to Motor-CAD to create a first approximation of the desired design.

Some parameters were undefined, forcing us to retrieve them in the literature (mainly following [2], or through geometrical calculations, and they are summarized in the Tab. 7.1.

The final design that will be tested is reported in figure below. It is important to note that, being in the design phase, and with the objective of finding the best stator cooling solution for this motor configuration, the presented schematic fully satisfies validation requirements.

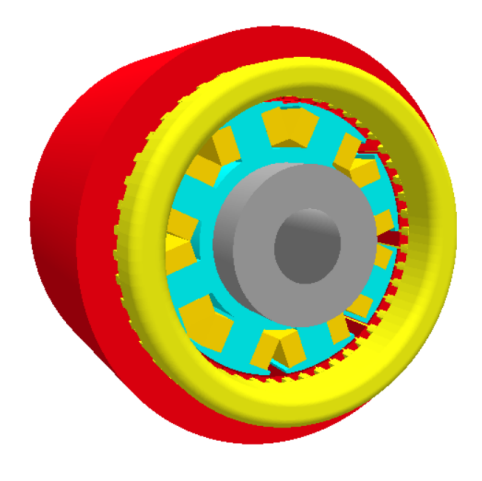


Figure 7.1. 3D view of the EESM in MotorCAD

Parameter	Motor-CAD Name	Symbol	Value [Unit]	
Stator slots	Slot Number	Q_s	48	
Stator bore	Stator Bore	D_s	116.62 mm	
Outer diameter	Housing Dia	D_e	209.7 mm	
Slot width	Slot Width	w_s	$3.58062 \mathrm{\ mm}$	
Slot depth	Slot Depth	h_s	15.17 mm	
Slot opening	Slot Opening	w_{so}	$1.16729~\mathrm{mm}$	
Tooth tip depth	Tooth Tip Depth	h_{so}	1.00 mm	
Tooth tip angle	Tooth Tip Angle	α_t	$5 \deg$	
Airgap length	Airgap	δ	0.7 mm	
Rotor slots	Rotor Slots	Q_r	8	
Pole width	Pole Width	w_p	14.3998 mm	
Pole depth	Pole Depth	h_p	15.5 mm	
Pole tip width	Pole Tip Width	w_{tp}	11 mm	
Pole tip depth	Pole Tip Depth	h_{tp}	4.5 mm	
Rotor coil width	Rotor Coil Width	w_{coil}	9 mm	
Rotor coil depth	Rotor Coil Depth	h_{coil}	14 mm	
Shaft diameter	Shaft Dia	D_{sh}	65 mm	
Shaft hole diameter	Shaft Hole Dia	$D_{sh,h}$	30 mm	

Table 7.1. Stator and rotor geometric input data from Motor-CAD

7.1 Thermal modeling (MotorCAD)

Thermal modeling of the EM is crucial to ensure a good understanding of heat distribution and to find a solution to ensure robust cooling while maintaining high motor performances.

This chapter will address motor thermal network modeling from MotorCAD in order to design an effective cooling system.

The thermal network in MotorCAD diverges the motor into discrete thermal nodes, each corresponding to EM components such as the stator core, windings, rotor, air gap, housing, and bearings. All heat transfer mechanisms, such as conduction, convection, and radiation, that develop between the motor components and the cooling system, are modeled through thermal resistances.

The complete machine is then divided by MotorCAD into its main components:

- Stator
- Rotor
- End Windings
- Air gap
- Housing
- Shaft and Bearings
- Insulation

In figure below is reported the visual thermal resistance schematization of our prototype with a basic housing configuration (round housing).

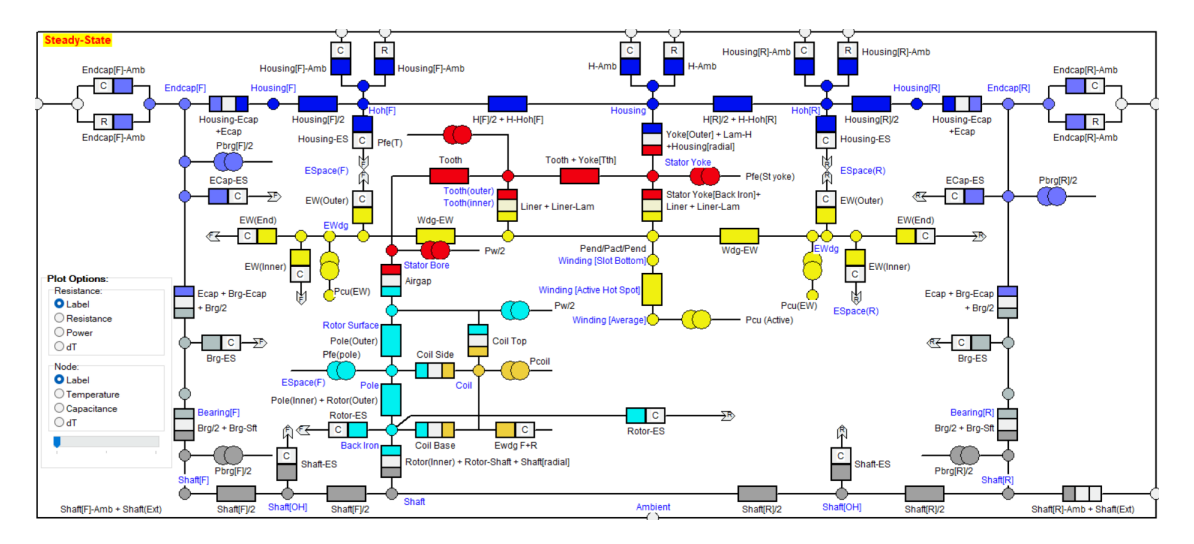


Figure 7.2. Thermal network base round housing configuration

In the next sections are shown the stator cooling solutions adopted for the present work, to underline the main differences in the MotorCAD thermal network.

7.1.1 Water Jacket Cooling

Considering the liquid jacket system, it is possible to note an additional line which is composed of an extra power source (pump) and a thermal resistance for the convection heat transfer.

7.1.2 Direct Slot Cooling with In-slot winding cooling

This configuration is conceptually reported in Fig. 6.5, but it only involves the integration of the cooling channel (or ducts) within the lower part of the winding slots of the stator (also known as *Stator Water Jacket*). The thermal network of this method is identical to

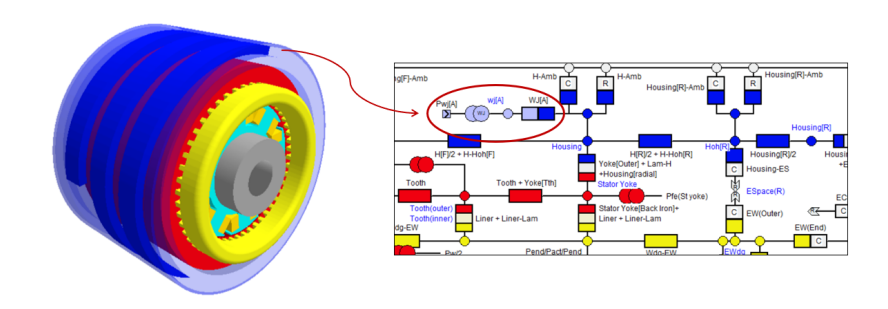


Figure 7.3. Thermal network WJ cooling configuration

the base configuration; the only difference lies in the fact that the thermal dissipation is modeled by a difference between the source power and the winding losses.

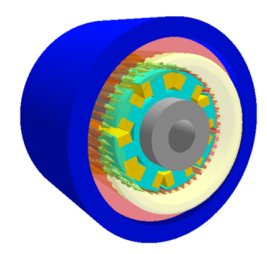


Figure 7.4. Direct Slot with In-slot winding cooling configuration

7.1.3 Direct Slot Cooling with In-slot winding cooling and stator ducts

This configuration is reported in Fig. 6.5. The addiction of stator ducts is believed to improve the cooling of the stator; these are integrated into the stator assembly and present different configurations depending on the needed configuration. For both ports (bottom of the windings and upper surface of the stator), the inlet and outlet ports are located at the two extremities of the motor and allow the coolant to flow in only one direction (from inlet to outlet). The thermal network presents an internal line that represents the cooling of the active part (stator core).

7.2 Losses computation (MotorCAD)

To ensure consistency between the MotorCAD model and the Ansys Fluent model, (adopted tool for CFD simulation), the main electromagnetic losses are calculated in MotorCAD through the "E-model", and then imported into the Ansys Fluent model as thermal inputs. Through empirical correlations findable in the literature, the losses calculated can be verified to ensure reliability of the method.

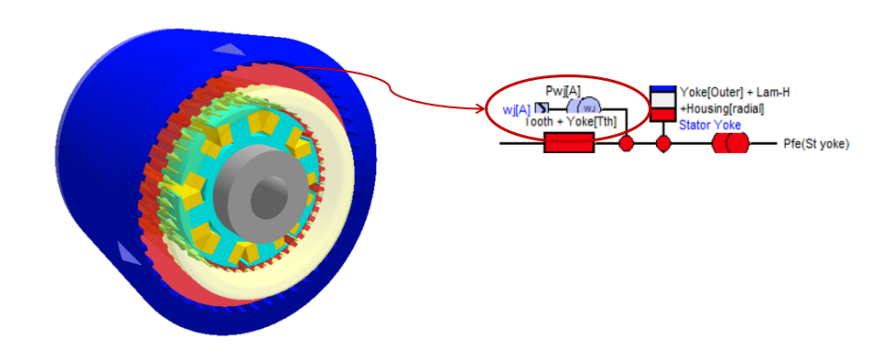


Figure 7.5. Direct Slot with In-slot winding cooling and stator ducts configuration

The analysis performed in this study refers to the *continuous operating mode* of the EM, corresponding to an operating speed of **4750 rpm** and a load of **80 Nm** Torque. *Peak mode*operation is not considered as limiting the maximum temperatures in the worst operating conditions is not the focus of the present work.

In Tab. 7.2 are summed the main loss contributions (not negligible) calculated by the E-model, in continuous mode.

Contribution	Motor-CAD Name	Symbol	Value [W]
Field DC Copper loss	Loss [Rotor Copper (Active)]	P_{exc}	628.8
Armature DC Copper loss	Loss [Armature Copper (dc)]	$P_{J_s,DC}$	1563
Armature DC+AC Copper loss	Loss [Armature Copper (dc+ac) (Active)]	$P_{J_s,B}$	918.9
Total stator back iron loss	Loss [Stator Back Iron]	$P_{Fe,bi,B}$	111.7
Total stator tooth loss	Loss [Stator Tooth]	$P_{Fe,t,B}$	143.7

Table 7.2. Losses contributions calculated by MotorCAD, in continuous mode

To ensure consistency in the model result, it is crucial to verify that the net heat transfer across the domain does not show any unbalance (net flux, neglecting the external HTC $\tilde{0}$. This can be verified in Ansys Fluent using the command *net heat transfer rate*, ensuring that the total heat extraction power equals the total power loss applied to the stator components.

Chapter 8

Methodology

The model was first created in SolidWorks to define the geometry of the EM's stator, labeled in SpaceClaim, and then imported into AnsysFluent for the fluid-dynamic simulation.

The thermal and electromagnetic effects of the rotor components were reproduced by incorporating a heat convection flow through the stator components which releases the equivalent heat generated by the rotor assembly, assuming operation under continuous mode conditions.

A fluid-dynamic simulation was performed for each cooling configuration, testing four different coolant volumetric flow rates (6-10-15-18 l/min), all with an inlet temperature of 65 C

Several simplifying assumptions were made to reduce computational cost while maintaining accuracy. The resulting electromagnetic losses calculated in the previous chapter are applied as input heat sources in the thermal model. In the fluid domain, a fully developed non-isothermal flow is assumed. Thin components, such as the slot liner and air layers, were treated using the thin-layer approximation findable in [22]. Furthermore, both the anisotropic properties of the slot and the endwings were modeled following the analytical model presented in [22]. Finally, all thermal properties were modeled as function of the rotor speed, but only considering the continuous mode operation.

8.1 Geometry definition - SolidWorks

The first step in creating the models involved using basic SolidWorks functionalities to construct the 3D geometry.

To align with the reality of the problem, all entire stator assembly, composed of cooling housing, stator lamination, and windings, is designed based on the initial specification and dimensions obtained in the previous chapter.

All geometries are strictly connected but not joined in a single solid to be able to extract the thermal flux in each single component.

As discussed previously, three main cooling strategies have been designed and tested:

• Water Jacket Cooling;

- Direct Slot Cooling with in-slot flow (called for simplicity *DirectSlotV1*);
- Direct Slot Cooling with in-slot flow and stator ducs (called for simplicity *Direct-SlotV2*);

To ensure consistency across the test simulated, all models have the same inlet flow area, equal to $S_{in} = 0.000260531m^2$; the air gap has not been changed with respect to the specification, even considering the presence of the sleeve in the last two configurations.

For each model, extra surfaces are created in correspondence with the inlets and outlet entrances, to ensure a correct interpretation of the fluid domain boundaries. These surfaces were then merged with the fluid domain (channel block) to ensure connectivity. The result is four main solid regions: Housing, Channel, Stator Lamination and Windings. An overview of the three 3D models (WJ, DirectSlotV1 and DirectSlotV2) has been reported in Fig. 8.1.

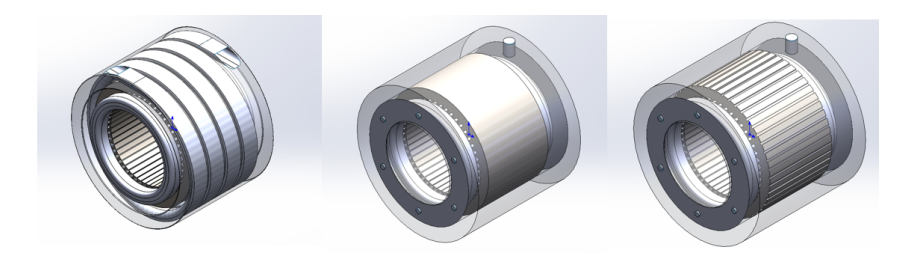


Figure 8.1. 3D model of WJ cooling (left), DirectSlotV1 (center), and DirectSlotV2 (right)

8.2 Geometry description - SpaceClaim

Once the 3D model in SolidWorks has been created, it was imported into SpaceClaim to categorize and organize the various components of the problem into specific groups.

These groups include:

- Inlets: flow entry points;
- Outlet: flow exit points;
- **Housing**: heat dissipation interface between the stator and the external environment;
- Stator Lamination: laminated iron sheets horizontally displaced and packet together (can be represented in a single block without losing much accuracy);
- Slot Windings: copper conductors placed in the stator slots;
- End Windings: part of the coils that extend outside the stator core;
- Flow Channel: domain region in which the coolant flows.

SpaceClaim was used in this context solely to assign appropriate names to the different parts of the domain to allow for a more clear communications with the Ansys Fluent environment.

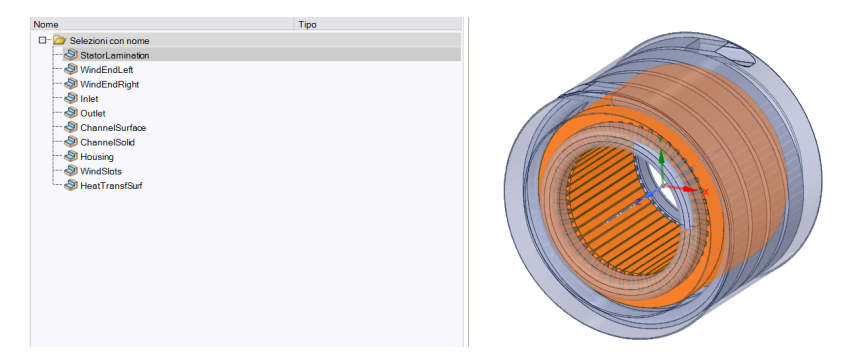


Figure 8.2. Assignment of domain parts in SpaceClaim, case of WJ cooling

8.3 CFD analysis - Ansys Fluent

8.3.1 Mesh generation

The first step involves the mesh mesh discretization as it plays a critical role in determining the accuracy and reliability of the simulation. Proper discretization ensures that the boundary layers and interaction regions are adequately captured, which is crucial for accurate representation of physical phenomena. To achieve this, local sizing was implemented to refine the mesh in critical areas; the following local sizing were applied:

• Inlets and Outlet: 2 mm

• End Windings external surface: 1.2 mm

• Slot Windings external surface: 1.2mm

• Fluid to solid interface: 1.5 mm

The geometry type has been chosen as "The geometry consists of both fluid and solid regions and/or voids"; this option enables the definition of regions containing different materials or states, ensuring accurate simulation settings.

A "Share Topology" function with a maximum gap distance of 0,2 mm has enabled us to ensure proper connections between the domains.

Then, boundary conditions were defined: the inlets ports were set as "Mass Flow Inlet", while the outlet port was set as "Mass Flow Outlet". Boundary regions were then defined to reflect the physical properties of the components, as the fluid domain was defined as "Fluid", while all other solid components were defined as "Solid".

Finally, a "Poly-hexacore" volume mesh was generated across the entire domain using the "Generate Volume Mesh" command. The aim is to produce a uniform and high quality

discretization suitable for the subsequent simulation stages. The wall Y+ in the turbulent flow domain was tried to keep it below 1 on the total channel surface, as it significantly affects the pressure drops and the calculation of the heat transfer.

All choices made in this step focused on finding the best compromise between the precision of the result and the computational time required for the simulation.

The mesh discretization of the WJ solution has been provided in the figure below.

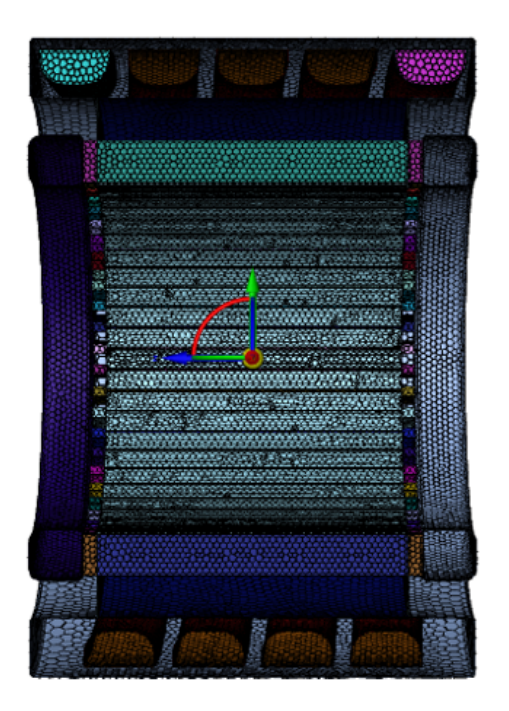


Figure 8.3. WJ mesh model discretization

8.3.2 Pre-processing: solver settings

This phase is crucial as it defines the problem physis, boundary conditions, and solver settings.

The "Energy" solver setting has been enabled to capture the heat transfer mechanisms; furthermore, the "Viscous (SST k-w)" turbulence model was selected to count the effect of a turbulent flow in the regions where it generates.

In the "Boundary conditions" panel, the inlet flow temperature of 65 C and the volumetric flow rate inlet value have been imposed for each simulation.

The influence of the rotor components has been reproduced by incorporating a heat convection flow through the stator components of value corresponding to the ratio between the total losses present in the rotor found in Tab 7.2, and the active surface area.

To account for the convection heat transfer between the outer walls and the environment, a common external temperature of 80 C has been chosen to ensure consistency between the models. It is important to note that the convective heat transfer coefficient h responsible for this heat transfer, has been found to be $3 - 7(W/m^2K)$, thus it can be considered negligible with respect to the other heat transfer mechanisms involved.

All material properties, corresponding to each component, have been provided by the supplier and are summarized in Tab. 8.1.

Component	Material	Type	Density [kg/m ³]	$C_p [\mathbf{J/kg}\mathbf{\hat{A}\cdot K}]$	Thermal Conductivity $[W/m\hat{A}\cdot K]$
Slot windings	Copper (anisotropic)	Solid	8978	381	anisotropic
End windings	Copper (anisotropic)	Solid	8978	381	anisotropic
Stator core	Electric-oriented iron	Solid	7650	460	anisotropic
Housing	Aluminum (Alloy 195 Cast)	Solid	2790	833	168
Cooling fluid	EGW 50/50 oil	Fluid	1051	3504	0.411

Table 8.1. Bill of Materials (BOM) used for simulation

The material modeling adopted in the simulation takes into account the anisotropic thermal behavior¹ of both the iron lamination and the copper windings.

Referring to [22], this anisotropy behavior can be modeled by treating the winding and slot insulation as a single equivalent material, whose effective thermal conductivity depends on the fill factor, assumed $k_{fill} \leq 0.65$. Following the analytical model proposed in the article, the resulting values, for an estimated fill factor of $k_{fill} = 0.55$, are 2.1 W/mK in the lower conduction directions and 142 W/mK in the others.

8.3.3 Convergence criteria

Before running the simulation, in the "Convergence criterion" section, all quantities related to the momentum equation were set to converge when the residual errors reached an order or 10^{-6} , while for the energy equation the convergence was imposed at 10^{-8} .

The simulation was then executed specifying a maximum of 1000 iterations, number considered sufficient to achieve the convergence of the solution. Each model reached convergence in 1.5 h conducted on a workstation with an AMD Ryzen 5 3500U with Radeon Vega Mobile Gfx 2.10 GHz.

8.3.4 Mesh dependence analysis

To evaluate how the number of mesh elements influences the simulation results, an iterative process was adopted involving several simulations with progressively refined meshes. The focus is to understand where further refinement in mesh quality no longer affects the outcomes. The parameters considered for this study are the heat transfer coefficient between the active cooling channel and the surrounding housing and the average coolant temperature inside the channel. These metrics were chosen to assess both the accuracy and reliability of the mesh refinement process.

¹e.g. thermal conductivity coefficient differs depending on the direction considered.

Multiple testes have been performed, each with the same coolant flow conditions $(Q_{in}=6l/m,T_{in}=65C)$ and progressively refining the discretization of the mesh.

In Tab.8.2, the details of the local refinements as discussed in section 8.3.1, while Fig.8.4 illustrates the influence of the number of cells on the simulated parameters, under fixed operating conditions.

Region	Element size [mm]					
	$8.4 * 10^5$ cells	$9.2 * 10^5$ cells	$1.0*10^6$ cells	$1.2*10^6~\mathrm{cells}$	$1.4*10^6$ cells	
Inlet and Outlet	3	2.5	2.3	2	1.5	
End Windings	2	1.8	1.2	1.2	1.2	
Slot Windings	2	1.8	1.2	1.2	1.2	
Coolant channel	2.5	2.3	1.8	1.5	1.3	

Table 8.2. Characteristic element size in the the main regions for five models with different total number of cells

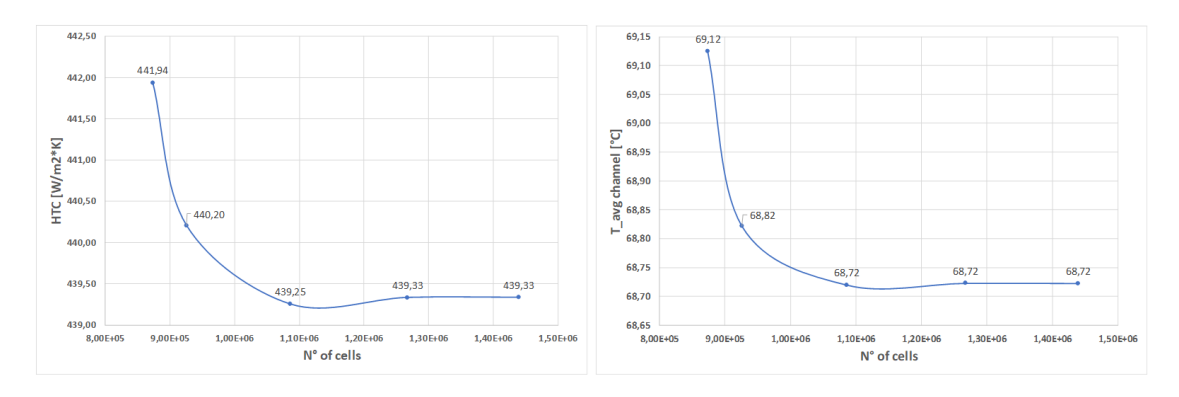


Figure 8.4. Mesh dependence analysis concerning the impact on Heat Transfer Coefficient and on the average coolant temperature in the channel for WJC strategy at fixed parameters and gradually increasing the mesh refinement

A good compromise between mesh accuracy and computational time has been achieved with the fourth configuration. The same dependence analysis has been performed for the other cooling strategies, with the same objective of balancing computational efficiency and result precision.

Chapter 9

Results and discussion

This chapter evaluates the simulation results of the three cooling strategies evaluated (WJ, DirectSlotV1, and DirectSlotV2), for the same operating conditions, same inlet port temperature and conditions, but with different volumetric flow rates. The comparison is made by evaluating some fundamental parameters: pressure drops along the channel, maximum temperature reached in the stator core, outlet temperature of the coolant, and heat transfer extraction for the stator core.

9.1 Analytical comparison

The pressure drop is crucial for good operating conditions, as it directly influences the exploitable work of the pump and therefore the overall efficiency; in this context, this value is calculated by simply subtracting the pressure at the inlet ports by the pressure at the outlet port $(p_{in} - p_{out})$.

Since the three cooling schemes have different overall channel lengths, a comparison must be made on the basis of the pressure drop, which corresponds to the power consumption of the coolant pump.

Gravitational effects were not considered, as the height difference between inlet and outlet ports had negligible values.

The pressure drop along a channel is mainly a function of the channel length; for this reason, the WJ configuration, having a higher channel length, is expected to have the highest pressure drops.

The maximum temperature is also a critical parameter for evaluating the thermal performance of the motor, as it determines the safe operating range of the machine, and this directly influences the reliability and efficiency of the EM. It is defined as the highest temperature reached within (in this case) the stator domain during steady state operation. This temperature is the main cause of insulation aging, increased resistive losses, and potential mechanical failure; thus, a proper cooling strategy allows limiting this temperature to a maximum of 150-200 C, depending on the EM configuration and power density.

The temperature of the coolant at the outlet, along with the effective heat extraction, are also crucial parameters, as they directly influence the general temperature of the motor and the temperature at which the coolant will have to be cooled for the next cycle. As we can see from Fig.9.4, the HTC values are fully aligned with the one reported in Tab.6.1.

A graphical comparison of the three cooling strategies based on the parameters discussed is reported in Fig.9.1, Fig.9.2, Fig.9.3, and Fig.9.4.

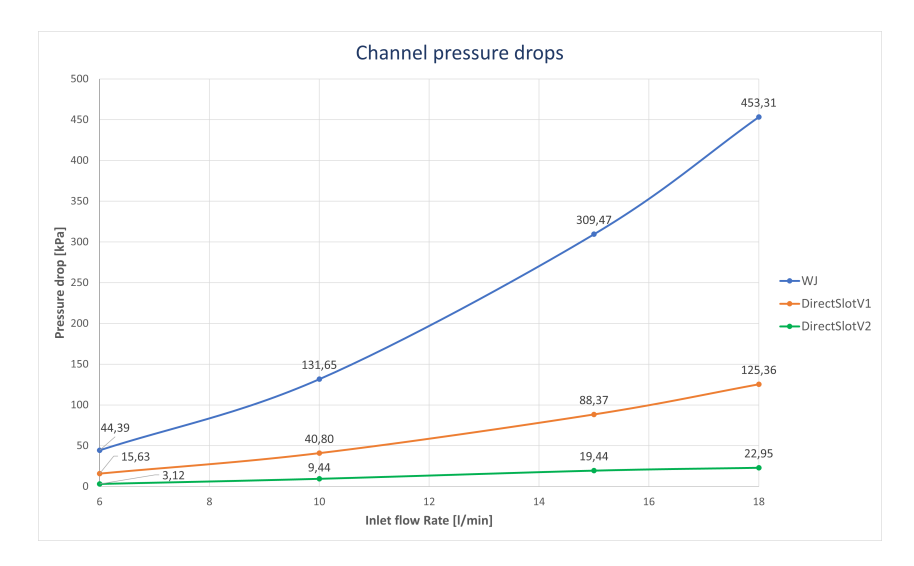


Figure 9.1. Pressure drop vs volumetric flow rate for each cooling strategy

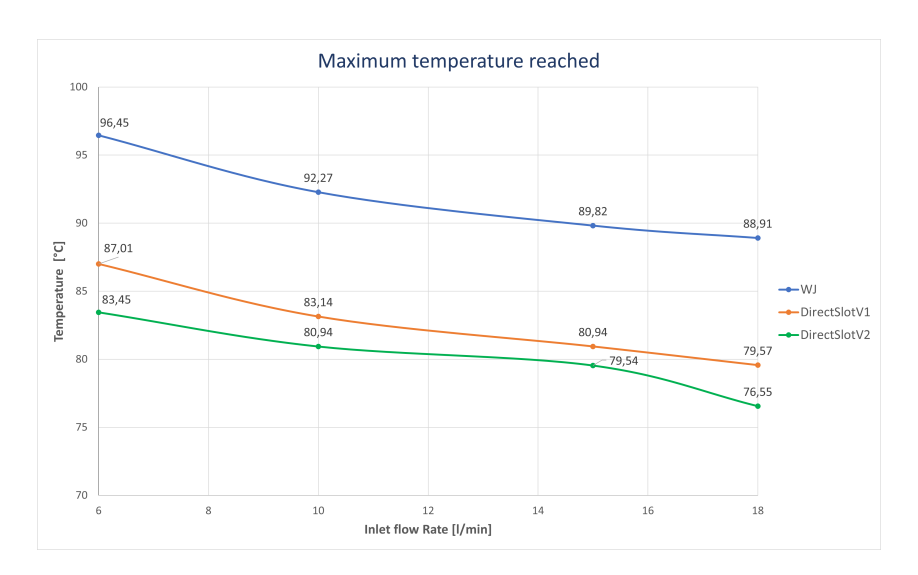


Figure 9.2. Maximum temperature vs volumetric flow rate for each cooling strategy

Analyzing the two diagrams, few considerations can be made:

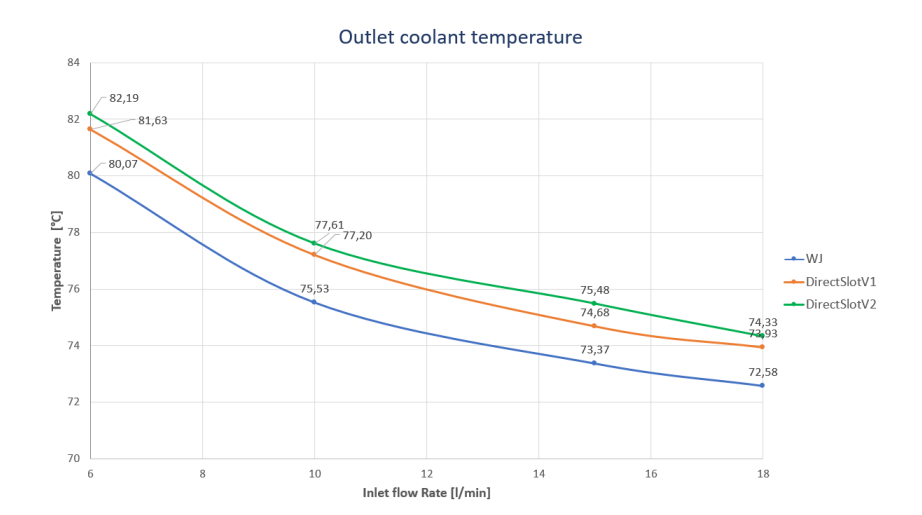


Figure 9.3. Outlet coolant temperature vs volumetric flow rate for each cooling strategy

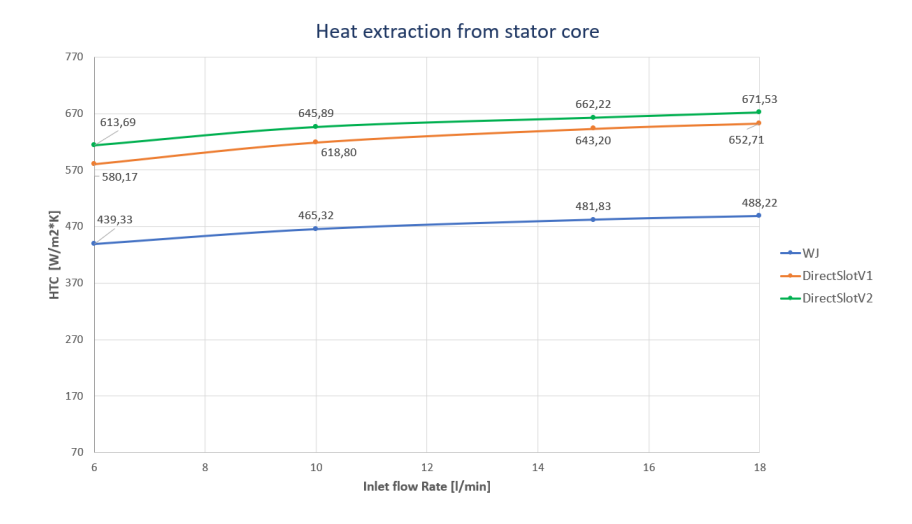


Figure 9.4. Heat extraction from stator core vs volumetric flow rate for each cooling strategy

- All configurations exhibit a clear decrease in temperature with higher flow rates, as the convective heat transfer is directly proportional to the volumetric flow rate;
- The WJ solution records the highest overall temperatures reaching a maximum of 96 C at 6 l/min, indicating that, although it is the most economical solution, it provides the lowest thermal efficiency;
- DirectSlotV2 shows the best thermal performance and it can be attributed to the higher contact points between the coolant and the heat sources inside the stator (e.g. better heat extraction);

- The pressure drop diagram confirms the hypothesized trend, as pressure drops increase almost quadratically with flow rate and WJ exhibits the highest pressure drop, reaching a maximum of $453\ kPa$ at $18\ l/min$; this is mainly due to the longer and narrower flow path;
- All cooling solutions respect the temperature limit imposed, but it emerges that DirectSlotV2 offers the best-trade-off between cooling effectiveness and hydraulic efficiency, despite its higher manufacturing costs and induced mechanical stresses.

9.2 Graphical comparison

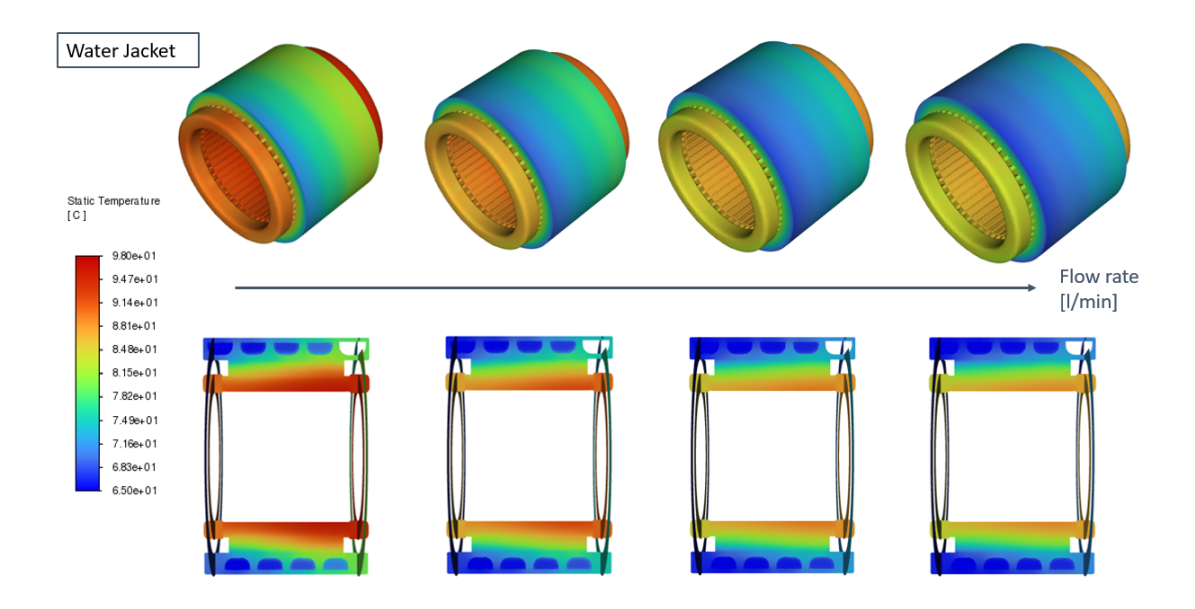


Figure 9.5. WJ stator core and housing temperature distribution varying the volumetric flow rate

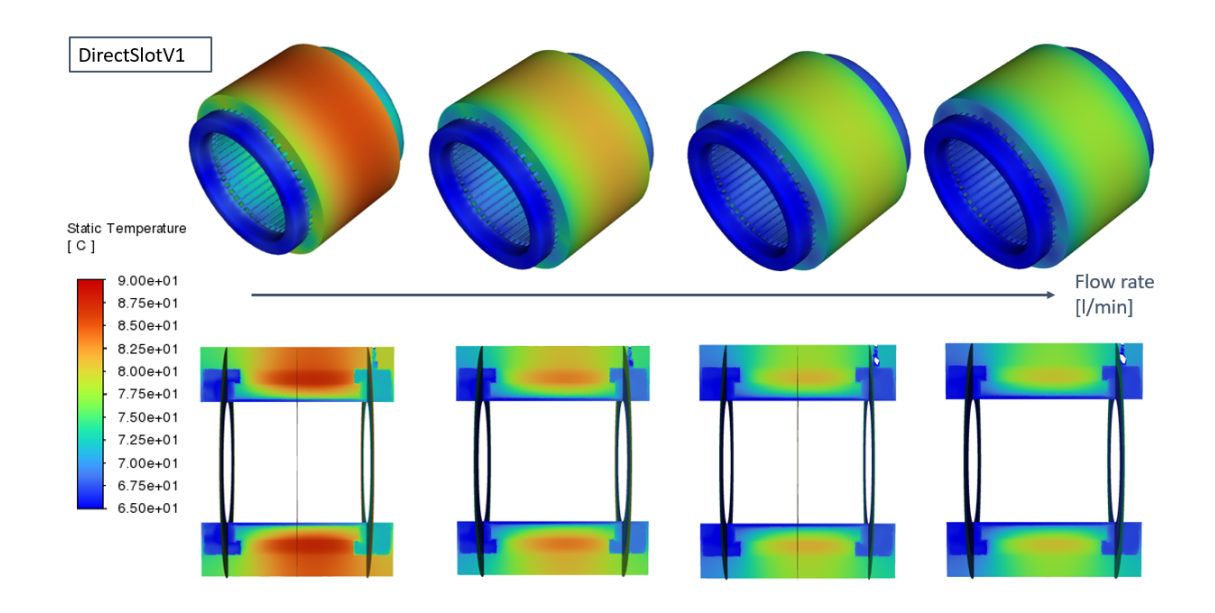


Figure 9.6. Direct SlotV1 stator core and housing temperature distribution varying the volumetric flow rate

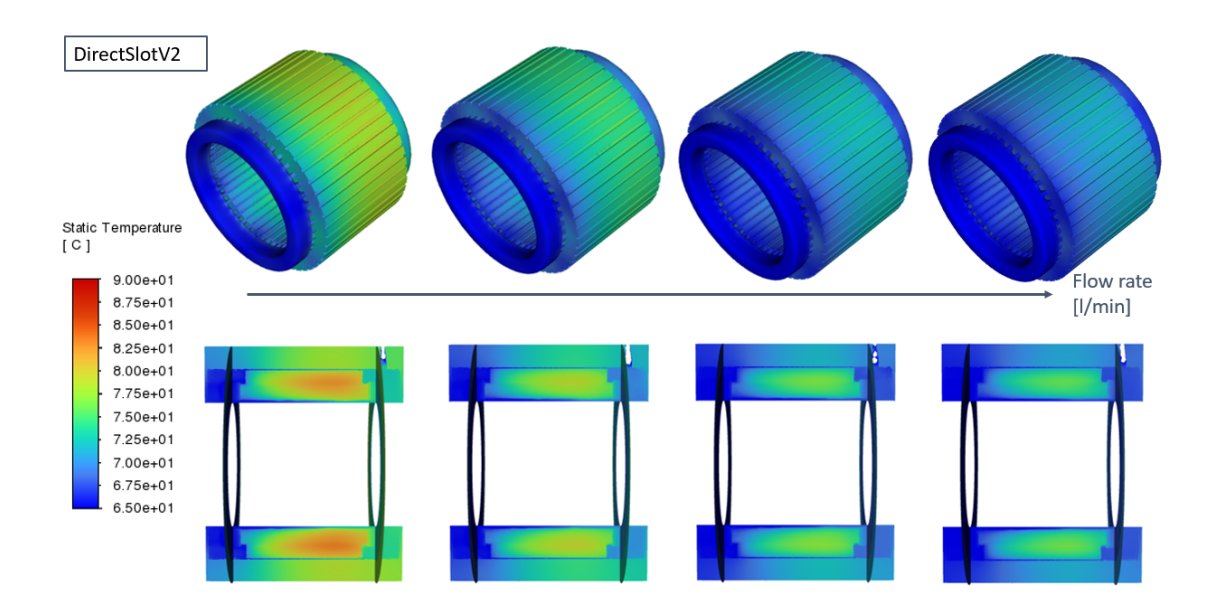


Figure 9.7. Direct SlotV2 stator core and housing temperature distribution varying the volumetric flow rate

Figures 9.5, 9.6, and 9.7 show the temperature field of the main EM components under

steady-state conditions for the three cooling configurations with an inlet flow rate increasing from 6 to 18 l/min. Based on the temperature contours provided, few considerations can be made:

- In the WJ configuration, as expected, the heat removal occurs mainly through the housing leading to higher stator temperature and localized hot spots as a consequence;
- The DirectSlotV1 configuration significantly improves the cooling efficiency with respect to the previous method, as the coolant interacts with the end windings and the lower part of the slot windings; although this, some thermal gradients still remain in the inner part of the stator core;
- The DirectSlotV2 configuration provides the most uniform temperature distribution and the lowest overall temperatures, underling that it represents the most effective solution among the one presented for heat dissipation within the stator components.

Chapter 10

Conclusion

Three liquid-cooled stator configurations for the proposed EESM prototype have been compared, with the objective of keeping the temperatures below the thermal limit while minimizing hydraulic losses. Loss maps were generated in MotorCAD, geometries in SolidWorks and SpaceClaim, and steady state CFD simulations were carried out in AnsysFluent; four flow rates (6-18 l/min) using a 50/50 EGW oil coolant at 65 C were tested.

The analysis focused on two indicators; maximum stator temperature and pressure drop. Among the investigated design, DirectSlotV2 achieved the lowest maximum temperature of the components and the most uniform temperature distribution.

The model presents some limitations such as the use of a steady state simulation, the simplification of the end-winding representation, and generic material properties; thus, it provides a solid foundation for future studies. Future work should include transient simulations, better end-winding modeling, optimization of the duct geometries, and other stator cooling strategies

Bibliography

- [1] I. E. A. (IEA), "Global ev outlook 2025, moving towards increased affordability," tech. rep., IEA, 2025.
- [2] G. M. e Alessandro Tacca, "Thermal design and control of a wound rotor synchronous motor for heavy-duty electric vehicles," Master's thesis, Politecnico di Milano, 2023/2024.
- [3] R. Bojoi, "Classification of e-motor solutions and torque production of ac e-motors." p. 16-24.
- [4] R. A. Di Gerlando, Appunti di macchine elettriche.
- [5] https://chargedevs.com/newswire/improved-motor-and-controller-gives-renault-zoe-greater range.
- [6] https://paultan.org/2021/09/06/renault-megane-e-tech-electric-up-to-470-km-range-android-automotive-os-26-driver-assist functions.
- [7] https://futurride.com/2023/09/15/byd-brings-seal-electric-sedan-to europe/.
- [8] E. M. Illiano, Design of a highly efficient brushless current excited synchronous motor for automotive purposes. PhD thesis, 2014.
- [9] F. P. I.-D. P. D. T.L. Bergman, A.S. Lavine, *Introduction to Heat Trasfer*. John Wiley Sons, 2011.
- [10] M. Polikarpova, "Liquid cooling solutions for rotating permanent magnet synchronous machines," Master's thesis, Mech. Eng. Lappeenranta Univ. Technol Lappeenranta, Finland, 2014.
- [11] Y. C. C.-J. D. W.-X. D.-M. P. Yaohui Gai, Mohammad Kimiabeigi, "Cooling of automotive traction motors: Schemes, examples, and computation methods," *IEEE*, p. 2 to 12., March 2019.
- [12] S. P. D. Staton, E. Chong and A. Boglietti, "Cooling of rotating electrical machines: Fundamentals, modelling, testing and design," *Institution of Engineering and Technology (IET) Energy Engineering Series*, 2022.
- [13] P. A. S. J. P. C. N. E. A.La Rocca, Z. Xu, "Thermal management of a high speed permanent magnet machine for an aeroengine," *University of Nottingham*, 2016.
- [14] D. A. H. R. Camilleri and M. D. McCulloch, "Predicting the temperature and flow distribution in a direct oilcooled electrical machine with segmented stator," *IEEE Trans. Ind. Electron*, 2016.
- [15] X. Z. G. D. L. J. S. D. Liu, C. and H. Zhang, "Experimental investigation on oil spray cooling with hairpin windings," *IEEE Transactions on Industrial Electronics*, 2020.

- [16] S.-C. Carpiuc and C. Lazar, "Modeling of synchronous electric machines for real-time simulation and automotive applications," 14 july 2017.
- [17] Globalspec, "Electrical equipment handbook." chapter 5 AC machine fundamentals.
- [18] L. B. H. C. J. Tang, B. Jiang and Y. Liu, "Observations of field current and field winding temperature in electrically excited synchronous machines with brushless excitation," *International Conference on Electrical Machines (ICEM)*, Valencia, p. 841 to 847., 2022.
- [19] W. U. B. U. A. H. M. S. Akbar, F. Khan and A. A. Azhari, "Performance analysis and optimization of a novel outer rotor field-excited flux-switching machine with combined semi-closed and open slots stator," *Energies VOl* 15, p. 7531, 2022.
- [20] W. Bader, "Control of electrically excited synchronous motor," Master's thesis, Universit A degli Studi di Padova, 2023/2024.
- [21] A. B. A. C. D. H. M. Popescu, D. A. Staton and J. Goss, "Modern heat extraction systems for power traction machinesâa review," *IEEE Trans. Ind. Appl.*, p. 2167 to 2175, June 2016.
- [22] E. A. G. S. T. L. Alessandro Acquaviva, Oskar Wallmark, "Computationally efficient modeling of electrical machines with cooling jacket," *IEEE*, p. 4 to 8., September 2019.
- [23] Y. J. Y. J. K. Chanyoung, S. Woohyuk and L. Tonghun, "Numerical and experimental analysis of a dual-channel electric motor housing cooling system," *Elsevier*, 2025.
- [24] J. W. X. X. F. B. Zhang, R. Qu and Y. Chen, "Thermalmodel of totally enclosed water-cooled permanent-magnet synchronous machines for electric vehicle application," *IEEE Trans. Ind. Appl. Vol 51*, June 2015.